INVESTIGATIONS OF CHITIN- AND CELLULOSE- BASED MATERIALS

by

Rebecca Winnick

B. Sc., Evergreen State College, 2012

A THESIS SUBMITTED IN PARTIAL FULFILLMENT OF THE REQUIREMENTS FOR

THE DEGREE OF

MASTER OF SCIENCE

in

THE FACULTY OF GRADUATE AND POSTDOCTORAL STUDIES

(Chemistry)

THE UNIVERSITY OF BRITISH COLUMBIA

(Vancouver)

December 2017

Abstract

Chitin plastic was fabricated from Dungeness crab shells. Chitin was purified from the shells, deacetylated, and then formed a gel in weak acid. The gel was poured into molds and then dried to leave behind a plastic film, which was strengthened by treatment with sodium hydroxide. Scanning electron microscopy (SEM) images of the dried film indicated that it adopts a layered structure. One sample batch was deacetylated for eight hours, and the other for twelve hours. The batch deacetylated for eight hours had superior characteristics, with a tensile strength of 93 ± 35 N/mm^2 and maximum strain of (7.5 ± 3) % while dry; after soaking in water for an hour, the tensile strength decreased to 7 ± 7 N/mm^2 and the strain at fracture increased to (31 ± 9) %. Contact angle experiments showed that the material is hydrophobic. Infrared (IR) spectroscopy confirmed a high degree of deacetylation in the final material. Results from IR spectroscopy and X-ray diffraction suggest a low degree of crystallinity in the material. This strong and waterproof chitin bioplastic is promising for use as packaging and for medical technology.

Additionally, a new type of polypyrrole-cellulose composite was developed. Polypyrrole was synthesized, mixed with an aqueous suspension of cellulose nanocrystals, and dried to a homogeneous black iridescent film. The film showed iridescence that is attributed to the chiral nematic structure characteristic of cellulose nanocrystal films. Surprisingly, the film was not found to have any conductive or capacitative electrical properties. When doped, these new composite materials could have interesting electrical properties owing to the chiral structure of the films.

Lay Summary

Chitin plastic was fabricated from Dungeness crab shells. Chitin is the main structural component of crab shells. The crab shells were subjected to several chemical treatments to obtain pure chitin, which was chemically modified to become chitosan. When the chitosan was submerged in weak acid, it became a gel, which was then dried to a solid plastic film, and strengthened by soaking in an alkaline solution. This strong chitin bioplastic is promising for use as packaging and for medical technology.

Additionally, a new type of polypyrrole-cellulose composite was developed. Polypyrrole is a synthetic conductive polymer, and cellulose nanocrystals can be extracted from trees. Polypyrrole was mixed with cellulose nanocrystals, and dried to a black iridescent solid film. The film was iridescent due to the twisted nanoscale structure of the film. Although polypyrrole is known to be a conductive polymer, the film was not found to be conductive.

Preface

Professor Mark J. MacLachlan supervised all of the work presented in this thesis. Dr. Thanh-Dinh Nguyen of the MacLachlan group at UBC was a collaborator, and House of Dosa restaurant supplied the raw material crab shells. Dr. Rick Carvalho and his Masters student, Bernardo Peres, kindly taught me how to use the Shimadzu strength testing machine in their lab. I conducted all experiments.

Table of Contents

List of Tables

List of Figures

List of Symbols

θ	angle of incidence
°	degrees
°C	degrees Celsius
M	molarity
vol %	volume percent
wt. %	weight percent

List of Abbreviations

CB	Chitosan Bioplastic
CB08	Chitosan Bioplastic with 8-hour deacetylation time
CB12	Chitosan Bioplastic with 12-hour deacetylation time
CNC	Cellulose Nanocrystal
EA	Elemental Analysis
FTIR	Fourier Transform Infrared Spectroscopy
POM	Polarized Optical Microscopy
PPy	Polypyrrole
SEM	Scanning Electron Microscopy
TEM	Transmission Electron Microscopy
TGA	Thermogravimetric analysis
UV/Vis	Ultraviolet / Visible
XRD	X-Ray Diffraction

Acknowledgements

Thank you to:

Thanh-Dinh Nguyen for the research concept.

Derrick Horne for SEM guidance.

Anita Lam for XRD analysis.

Dr. Rick Carvalho and Bernardo Peres for help with Shimadzu strength tester.

House of DOSA for providing Dungeness crab shells.

Pei-Xi Wang for moral support.

Stacy Winnick for editorial support.

Mark MacLachlan and the MacLachlan group, for inspiring and supporting me along the whole journey.

And to Vancouver for being a great place to live!

Chapter 1 – Introduction to Bioplastics and Chitin-Based Materials

1.1 Biopolymers

Multiple types of biopolymer are essential for life in every organism. Biopolymers are long chains of molecules linked together, created inside cells. All living cells contain DNA and RNA, which are polymers of nucleic acids, and polypeptides, which are long complex structures of amino acids. DNA is the blueprint for life and RNA reads the blueprint; together, they instructs the creation of polypeptides and proteins that perform an abundance of jobs in the cell.

Sugar and starch polymers function as energy storage molecules for autotrophic plants. Plant sugars and starches in turn become the food source for herbivores and fungi. Cellulose polymer is found in the cell walls of plants, and chitin in the cell walls of fungi. Cellulose and chitin are structural polymers that are strong and flexible to encase the contents of the cells. Since plants and fungi have no skeletons, their forms are determined by these polymers.

Chitin also occurs as a structural polymer in insects and crustaceans. Although they have typical animal cell walls composed of non-polymeric lipid crystals, chitin is a major component in their exoskeletons and shells. The shells of crustaceans are made of three main components: chitin, proteins, and calcium carbonate. Crustaceans secrete chitin polymers which create the general shape of the shell – the proteins guide this construction.[1] Calcium carbonate ions are filtered from ocean water and secreted by the crustaceans during shell formation to precipitate and harden among the chitin. Chitin gives the shells flexibility and form, while the calcium carbonate lends hardness and extra strength.

Another type of biopolymer, polyhydroxyalkanoates (PHAs), are created by bacteria. PHAs are thermoplastic linear polyesters that can be heat-processed, and have material

properties similar to the synthetic plastic polypropylene.[2] PHAs can be "farmed" at industrial scales – bacteria ferment glucose or lipids into PHAs. Different types of stressful conditions can induce the bacteria to create more PHA. Several different bacterial strains are used to produce PHA with different properties.

The most common starting materials for bioplastics are cellulose, chitin, and PHA.

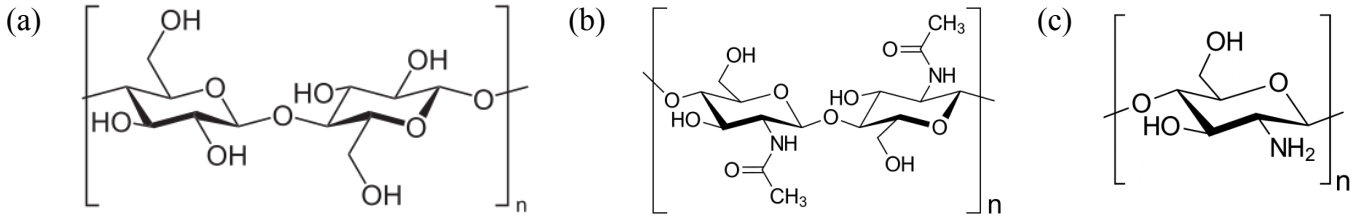

Figure 1-1 Structure of (a) cellulose, (b) chitin, and (c) chitosan

1.2 Bioplastics

Bioplastics offer a green alternative to traditional petroleum-derived plastics. Synthetic plastics made from petroleum pose a number of environmental problems. The production is not sustainable, because the Earth has a limited supply of petroleum, and they are generally not biodegradable, because no natural bacteria exist that can break down synthetic polymers. Non-biodegradable waste becomes persistent environmental pollution.

On the other hand, bioplastics are biodegradable and they can be created using renewable resources. Over the past few decades, many types of biodegradable, compostable, and/or sustainable bioplastics have arrived at the research arena and the market. The varieties include cellulose, chitin, starch (often from corn), PHA, PLA [poly-lactic acid; $(\text{-CH}(\text{CH}_3)\text{-CO-O-})_n$], PCL

(polycaprolactone), collagen and other polypeptides. They are either derived from the bodies of plants or animals, or farmed as microbial byproducts.[3]

PLA bioplastics are among the most common of these, and are used in medical equipment, packaging, and disposable cutlery. PLA is derived most commonly from corn, but can also be produced from potatoes, wheat or beet sugar.[4] The starch from the feedstock is converted into dextrose, followed by fermentation into lactic acid. The isolated lactic acid monomers are then polymerized through ring-opening reactions or by direct polycondensation to create PLA pellets.[5] PLA is a thermoplastic with high strength and modulus, but melt processing is difficult because the structure degrades at the high temperatures required (185–190 °C). To enable melt processing, polycarbonate and polyethylene blends are occasionally used. Blends with both synthetic and other natural polymers have been used for a variety of purposes.[6] With regard to environmental concerns, these pure corn plastics are biodegradable, but not recyclable. PLA products can pollute the recycling stream if they are accidentally recycled.[7]

One major drawback of PLA plastic is that when agricultural areas are expanded to grow more corn feedstock, this land-use change leads to increased greenhouse gas emissions. Though using corn-based plastic prevents the greenhouse emissions caused by petroleum-based plastics, it is counterproductive when it creates a similar amount of greenhouse emission due to changed land-use. To avoid this problem, Piemonte & Geroni stress the importance of using waste biomass for the corn bioplastic industry, or using corn grown on previously degraded or abandoned agricultural lands.[8]

Not all corn-based bioplastic is PLA: Aithani & Mohanty created a very sustainable bioplastic from corn gluten meal, a byproduct of the corn-based ethanol industry.[9] (Of course, the production of this ethanol requires agricultural farmland to grow corn, which affects greenhouse

emissions). The corn gluten meal was plasticized with glycerol and ethanol, denatured with guanidine hydrochloride, and blended with synthetic poly (ε-caprolactone) to create a biodegradable plastic that is stronger and more elastic than high-density polyethylene (HDPE).

Rather than converting starch to PLA, it can also be plasticized without chemical conversion. Cereals, legumes, and tubers store their energy as starch polymers. Starch can be processed to create bioplastic by adding flexibilizers and plasticizers such as sorbitol and glycerine.[5] The result is a thermoplastic material moldable by heat and mechanical energy, which can be used in packaging and other industrial applications including injection moulding, blow moulding, film blowing and foaming.[5] However, starch-based plastics continue to have problems with mechanical properties, moisture sensitivity, brittleness and processing difficulty. In spite of these disadvantages, starch is still quite commonly used.[3]

Some bioplastics are created from microbial sources. The most widely produced are PHB (poly(3-hydroxybutyrate)), PHA, and their derivatives, with PHA being the most common. The growth conditions and recovery of plastic particles from microbial biomass are complex and costly to create and maintain.[10] Because production of PHA is more expensive than traditional synthetic plastics, recent research has focused on reducing costs through use of cheaply obtainable waste-stream feedstocks for the bacteria. Fortunately, the bioreactors do not require sterile conditions. The market for PHA-based plastics is expected to grow a lot in the coming years, as technology improves, and governments place stricter regulations on the use of non-biodegradable plastics. PHA has great potential for packaging, food-wrapping, medical, and agricultural applications.[2]

Researchers are also investigating methods to create bioplastics from whey protein. Fifty million tons of unprocessed whey waste is produced per year, so it is an abundant resource.[11] Whey plastics are useful for packaging applications because they have excellent oxygen barrier

capabilities; however, they tend to be stiff and brittle. Sharma & Luzinov made composite plastics by mixing whey with natural latex or egg albumin protein for enhanced mechanical properties.[11]

Materials chemists continue to seek innovative ways to create bioplastics with versatile characteristics and low processing cost. The end goal is for all plastic to be biodegradable and sustainably produced: harmful and wasteful synthetics will no longer be used.

1.3 Chitin & Chitosan Background

Chitin is formed by crustaceans as they grow. Proteins guide the conformation of the flexible and strong chitin polymer, and calcium carbonate mineralizes within the chitin scaffold to toughen the shell.[12] Chemically and structurally, chitin ([poly-β-(1,4)-N-acetyl-D-glucosamine]) is similar to the cellulose polymer (Figure 1-1), which is why it is useful to compare cellulose and chitin as building blocks for bioplastics. They both form crystalline nanofibers that are held together by strong hydrogen bonds. The acetyl group on chitin can be removed after treatment with strong base at high temperature, yielding the chitin derivative *chitosan*. During this deacetylation process, some of the structural hydrogen bonds are also weakened.[13] The relative amount of acetyl groups removed (leaving amine groups) is known as the degree of deacetylation (DD).

Chitin- and chitosan-based materials are used in many applications including bioplastics, food, biotechnology, pharmaceuticals, and even gene therapy.[13]

1.4 Bioplastics from Chitin and Chitosan

Chitin is a promising ingredient for use in bioplastics. It is the second-most abundant biopolymer in the world (after cellulose), and the main structural component in the shells of ocean-dwelling crustaceans such as crab and shrimp. 150,000 tons of chitin-rich waste is produced annually by the seafood industry worldwide.[14] Disposing of this waste is a burden on the industry, as there are not yet many commercial uses for it. Making bioplastic from this waste in a cost-effective way can benefit the seafood industry by reducing waste-disposal costs. Chitin-based bioplastic also has a significant advantage over plastics made from corn. Corn must be grown in fields, but chitin waste is already available.

Chitin- and chitosan-based materials have both been shown to have antimicrobial[15] and even wound-healing properties. When Huang et al. used chitin-fibre fabric bandages for wound covering, the healing was accelerated compared to normal surgical gauze.[16] The anti-microbial and wound-healing effects make chitin/chitosan bioplastic an attractive option for food packaging applications, and various medical applications such as surgical implants or packaging bags for sterile items. Chitosan is non-toxic and non-allergenic. Nunes et al. used chitosan-blend films to protect white wine, and were able to preclude use of the preservative sulfur dioxide because the chitosan complexed stray metals, prevented oxidation, and prevented microbial growth.[17]

In the current work, we have developed a strong water-repellent chitosan bioplastic formed by dissolving chitosan in acetic acid, drying to a film, then strengthening by NaOH treatment. Gartner et al. employed a similar method to create films in 2011.[18] Although they reported the moisture content of the films, they did not comment on the swelling or water-proof behavior of films before and after base treatment. They measured the storage modulus (E) of their films but no

other mechanical properties. Their report offers an in-depth study of the chitosan self-association network.

There are some other examples of chitin- and chitosan- based plastics that have been reported in the literature. In 1996, Xu & McCarthy made chitosan films from acid-dissolved chitosan, which were neutralized with NaOH.[19] They then reacetylated the films and studied the chemical differences, and showed that the films were biodegradable. They did not measure the mechanical or swelling properties of the films. Ifuku et al. (2013) developed chitosan films reinforced with surface-deacetylated chitin nanofibers for increased strength.[20] The films were shown to have antifungal activity, but water-stability was not mentioned. Jin et al. made transparent and flexible chitin bioplastic; however, the method requires the harmful solvent hexafluoro-2-propanol, and can only be made with beta-chitin, which is a rare form of chitin found in few organisms.[21]

Elsabee & Abdou[22] have reviewed progress towards making edible protective food coatings from chitosan. All materials they examined suffer from high water-vapor permeability due to hydrophilicity. Tan et al. blended hydrophilic chitosan with synthetic hydrophobic polyethylene to address the water-vapor permeability issue.[23] Duan et al. made clear chitin films with effective gas-barrier properties using a NaOH/urea solution and freeze/thaw cycles to dissolve the chitin without deacetylation.[24] In one creative application, a chitosan/glycerol blend edible film was coated with thyme essential oil for an antimicrobial effect in meat packaging.[25] A chitosan coating also showed anti-microbial action when used as a preservative on salmon.[26]

Chitosan fibers have even been used in clothing. The antimicrobial properties of chitin help to inhibit odors in the commercial product Crabyon.

1.5 Background on Mechanical Properties

Measurement of mechanical properties of solids has many established standard methods. One test that can provide a variety of data uses a machine to pull on a material slowly until it breaks, measuring the force applied during the process. When running multiple tests of the same material, it is important that the size and shape of the samples are identical, because total mass has an effect on the amount of force needed to pull it apart. Notches are often cut uniformly in the center of the sample to make sure the break happens in the middle every time, rather than breaking where the machine grips the sample.

Data are plotted on a graph of stress versus strain. As the two grips on the sample move apart at a constant speed, both stress and strain vary depending on the character of the sample. Strain describes the deformation, or how far the sample has stretched. In this paper it is reported as percent strain, which is the percent the sample has stretched beyond its original length. Stress is reported in units of force, and describes how much force is exerted on the sample by the grips as they move apart at a constant rate.

The ratio between stress and strain, or the slope of the line, is known as Young's modulus and is a measure of stiffness. Materials are considered linear with regard to Young's Modulus if a Hooke's Law can be applied to the initial slope of the stress-strain curve. Hooke's law $F = kX$ relates stiffness (k), to stress (F) and deformation (X). After a plastic deformation occurs, materials lose their linear response.

Of course, no material yields a perfectly straight line, so it is sometimes more convenient to use the measurement of "max slope." Max slope may be qualitatively determined by overlaying a straight line on the graph, adjusted to lie over the section that appears the steepest. The slope of this line is used to determine the "max slope" measurement (illustrated in Figure 2-2).

Plastic deformation occurs mainly in plastics, when some bonds in the twisted polymers break and the entangled regions stretch out along the strain axis. This event often happens quickly and leaves the material in a weakened state. A plastic deformation is characteristically observed as a bump in the graph, the peak of which is known as the yield point, followed by a decrease in slope.

The speed at which the sample is pulled apart is adjusted by the operator. Slower pulling tends to allow for a plastic deformation to be observed, whereas faster pulling may lead to a swift break. If gradual deformation is allowed to occur, the sample will generally break at a higher force load.

The ultimate tensile strength (UTS) is the single point of the test at which force is the greatest. In a very brittle material, the UTS will be the same as the breaking point. In more flexible substances, the UTS will be a point of weakening but not breaking – the slope will become negative as the material relaxes before the breaking point is reached.

Figure 1-2 illustrates these definitions using a labeled stress-strain curve.

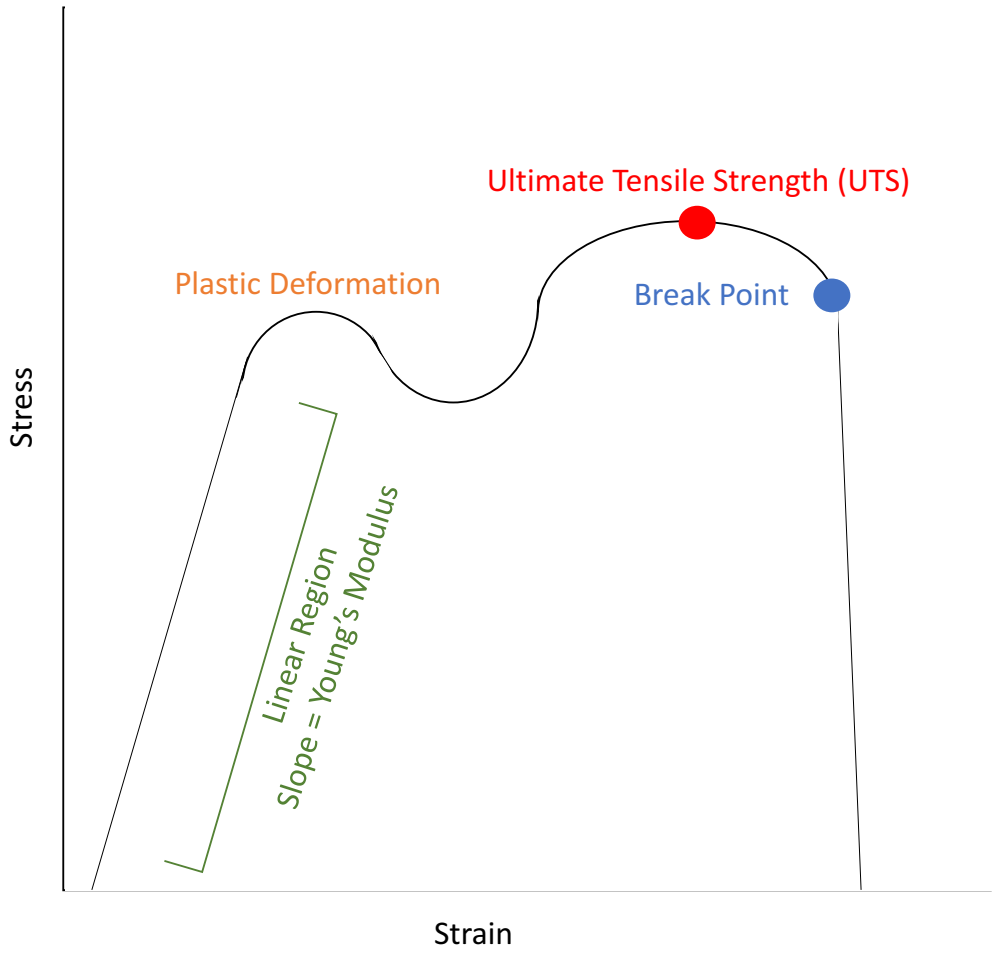

Figure 1-2. Illustration of mechanical properties using a stress-strain curve.

1.6 Goal of this Thesis (Chitosan Project)

The goal of this thesis was to develop and characterize a strong water-repellent chitosan bioplastic. In conducting this research, new bioplastic films were prepared by dissolving crab-derived chitosan in acetic acid, drying to a film, then strengthening by NaOH treatment. The material was characterized by UV/VIS, FT-IR, SEM, TGA, EA, XRD, strength testing, swelling testing, and contact angle testing. I succeeded in developing a reproducible synthesis of water-stable, strong, and transparent chitosan films.

Chapter 2 - Strong Waterproof Chitosan Bioplastic

2.1 Method Development

I experimented with a variety of chitin bioplastic preparations before arriving at the preferred method described in section 2.2. Initially I experimented with re-acetylated chitin films made by removing acetyl groups from the chitin polymers, and then adding them back on. The end products were interesting and occasionally very strong and water-resistant, but the results were never as consistently reproducible as the NaOH-strengthened chitosan bioplastic.

To make the reacetylated bioplastic, crab shells were first purified into chitin with acid and base, and then deacetylated with strong NaOH according to the methods described in section 2.2. After various times of deacetylation, the reaction progress was checked by taking a small piece of sample from the reaction beaker, rinsing it in water, and then submerging it in an excess amount of 1 vol% acetic acid. When chitin is deacetylated to become chitosan, it becomes soluble in acetic acid. This is due to interactions of chitosan's basic amine group with the acetic acid. When the samples dissolve, the acetic acid solution becomes a homogeneous clear gel. Fully dissolved samples were deemed sufficiently deacetylated, and ready for the reacetylation procedure. Under-reacted samples would bubble and swell, but not dissolve. There was some variation depending upon the batch, but samples started being able to dissolve sometime between 6 and 8 hours. After reacting much longer than around 12 hours, the material would start to turn brown. In general the samples that dissolved in 1 vol% acetic acid and did not turn brown had the greatest chance for success in the subsequent stages.

When the deacetylation reaction was halted, the chitosan samples were rinsed in water until the rinse water had neutral pH. One unusual effect was observed at this step. When rinsed by

soaking in neutral tap water or DI water, after a few minutes the samples would start to slowly release tiny bubbles that would adhere to the surface of the sample. It seemed that these bubbles would be generated indefinitely, because even after spending the night in a beaker of water with a stir bar, bubbles would continue to form over the following several days. Coinciding with this, the rinse water never reached its original neutral pH. In a still beaker, the water near the surface was neutral when tested with a pH strip, but touching the pH strip to the sample itself gave an alkaline reading. The samples remained alkaline after several days of soaking and changing the rinse water every day, so the pH was unlikely to be affected by any residual NaOH on the sample. The alkalinity may have been a result of the reaction that released the bubbles. The nature of this reaction is not certain, nor was it explored further, as a different experimental procedure was eventually chosen.

After rinsing, the chitosan samples were allowed to air-dry completely, usually lyophilized to remove excess water, and then reacetylated with acetic anhydride. They were cut into pieces less than 1 cm^2, and submerged in acetic anhydride in a closed vessel with stir bar overnight, enough time to ensure the reacetylation continued to completion. The reaction proceeds through the nucleophilic attack of the unprotonated primary amino group of chitosan on one of the carboxyl groups on acetic anhydride.[25]

When removed from acetic anhydride, the flakes were dried under ambient conditions in a fumehood. The next step was the novel part of this procedure: The samples could be dissolved in pure water. Similar to their deacetylated precursors, the reacetylated samples dissolved by turning to a clear viscous gel homogenously mixed within the solution. Notably, these reacetylated samples could dissolve in pure water rather than only in the acidic solution. This is a phenomenon

not previously reported in the literature. After the solution dried in a petri dish, films formed that were occasionally quite strong and waterproof.

It is remarkable that this reacetylated chitosan, chemically similar to chitin, could dissolve in water while the chitin purified directly from crab shells was so stable in water As previously noted, the original chitin also appeared to decompose somewhat in water. This change in characteristic is likely due to disruption of the hydrogen bonds holding the polymer together in chitin fibrils, which happened during the deacetylation process.

At this point in the research, a challenge posed itself: the water dissolution step did not always work. Sometimes, the samples would simply swell without dissolving, or not swell at all. Although the procedure was repeated many different times, with different modifications and controls on the variables, the complete dissolution was never reproducibly achieved, and indeed appeared more elusive the more often it was attempted. The conditions that were experimentally varied were crab shell species (Dungeness (*Metacarcinus magister*) vs. king crab (*Paralithodes camtschaticus*)), deacetylation temperature (75, 80, and 85 °C), deacetylation time (6 to 13 hours), air-dry vs. lyophilize before reacetylation, and air-dry vs. lyophilize after reacetylation.

When the samples did dissolve, and were dried into films, one final test remained. Were they water-stable? A few of the samples were hardy, did not swell much in water, and were difficult to tear with the fingers. One such sample, the strongest, was even created from brown material, made that color by an extra-long deacetylation time. Unfortunately, large batches of such samples were never achieved. Some of the films at this point would only shrivel and dissolve in water.

If this strong waterproof reacetylated chitosan bioplastic could someday be reproduced in further research, it would be ideal. These films are much preferable to the films that can be made from simple deacetylated chitin – when the deacetylated chitin is dissolved in acetic acid and dried,

it does make a film, but it is not water-stable. Eventually, it was found that those films could be made more waterproof by soaking in a weak NaOH solution, as described in section 2.2 below. However, that process causes the films tend to shrink during the NaOH soak, resulting in wrinkles.

2.2 Experimental Methodology

2.2.1 Sample Preparation

Dungeness crab shells were sourced from a local seafood restaurant. The shells (not including legs) were washed with soap, rinsed with cold water, then soaked in 5 wt. % NaOH at 80 °C for 6 h to remove exterior hairs and proteins from within the shell. After rinsing and scrubbing, the shells were immersed in 2 vol. %, then 5 vol. %, then 7 vol. % HCl to dissolve all the calcium carbonate. The concentration of HCl was increased stepwise in order to reduce damage to chitosan fibres. Each HCl soak was continued for 8 hours or until the solution stopped bubbling. This stepwise method was followed because it was found that immediately exposing the shells to 7 vol. % HCl caused visible damage to the material. Therefore, the concentration was gradually increased up to 7%, and after soaking in the 7 vol. % HCl, higher concentrations of HCl ceased to cause the observable bubbling effect, signaling the complete removal of $CaCO_3$. Red astaxanthin pigments were destroyed by the acid, and the resulting pure chitin films were white, strong, and flexible. All soaking solutions were used in excess to completely submerse the shells.

Deacetylation refers to the removal of acetyl groups from the chitin polymer. Chitin shells were cut into strips, then heated in 50 wt. % NaOH at 80 °C. The longer the deacetylation time, the more acetyl groups are removed, turning the chitin monomers into chitosan monomers. Two batches of chitin were deacetylated to different degrees, one for 8 h and the other for

12 h. Due to feedstock and labware limitations, only two batches were created, to ensure that there would be plenty of material for creating enough sample films for each batch. 8- and 12-hour deacetylation times were chosen because they worked well in earlier trials. In those trials, smaller samples were deacetylated for 5, 6, 7, 8, 9, 10, 11, 12, and 13 hours, and then put through the entire film-drying process. Eight hours was the shortest processing time that reliably yielded material that was sufficiently deacetylated to dissolve in 1 vol% acetic acid during the next step. Twelve hours was the longest processing time that did not appear to degrade the samples at the time of testing. The chitosan films made from the batches discussed here are henceforth referred to as CB08 and CB12.

The deacetylated shells were then rinsed and stirred with several changes of water over several hours until the pH of the rinse water was almost neutral. It was found that after extended periods of rinsing and soaking, the shells would slowly emit bubbles, and the rinse water was persistently slightly alkaline.

When fully rinsed of NaOH, the solid shells were dissolved in 1 vol% acetic acid. Sonication was used to aid dissolution. Most of the chitosan dissolved to form a clear gel, and remaining solids were removed via centrifugation. The minimal effective amount of acid solution was used to ensure that the gel was fully dissolved and pourable. This amount varied, but was roughly 1 mL liquid for 30 mg solid. Ifuku et al. (2009) describe how acid can solubilize chitin by cationizing the amino groups on the fiber surface, causing the fibers to fibrillate and drift apart.[26] The same principle is at work when dissolving chitosan.

Chitosan gel was poured with ~1 cm thickness into petri dishes, and left to dry over 2 weeks. The resulting films were floppy, plastic-like, and broke when folded over and creased. They also broke easily when pulled laterally. In contact with water, the films curled, swelled, and

dissolved. The surface was sensitive to moisture: a small piece of film is placed on the palm of the hand twisted and curled as a reaction to the moisture. Thus, to protect the films from the effects of moisture, they were then soaked in 0.5 M NaOH for 8 h then air dried. After this final treatment with base, the films were tougher and no longer dissolve in water. Rather, the water beaded up and rolled off the surface, indicating they are hydrophobic.

2.2.2 Experimental Details

All chemicals were purchased from Sigma Aldrich or Alfa Aesar and used as received. A Varian Cary 5000 UV-Vis-NIR Spectrophotometer was used to collect transmission spectra for the films. Thermal decomposition was measured with a Perkin Elmer Pyris 6 Thermogravimetric Analyzer (TGA). FT-IR spectra were collected with a Perkin Elmer Frontier FT-IR Spectrometer. Stress and strain were tested with a Shimadzu instrument using TrapeziumX software. The X-ray Diffractometer used was a Bruker D8-Advance with Bragg Brentano configuration, copper Ka1 & Ka2 radiation source, nickel filters, LynxEye detector, and slits 1 mm divergent, 8 mm anti-scatter, 2.5˚ soller. A Hitachi S-4700 Field Emission SEM was used to collect electron microscopy images, of samples that were sputter coated with 8nm of platinum/palladium. The equipment for testing contact angle is a custom setup at FP Innovations on the UBC campus. Elemental Analysis was performed by staff at the UBC chemistry department.

2.3 Results

2.3.1 UV/Visible Spectroscopy

To the eye, the CB08 is completely clear, while the CB12 is transparent light orange. The CB12 had a longer deacetylation time, so the orange color may be due to prolonged heating of chitosan that led to partial decomposition. Spectrophotometry data shows that both samples are opaque in the UV region of light (below 400 nm) (Figure 2-1). If chitosan bioplastic was used as food packaging, this characteristic would help protect food from UV light radiation.

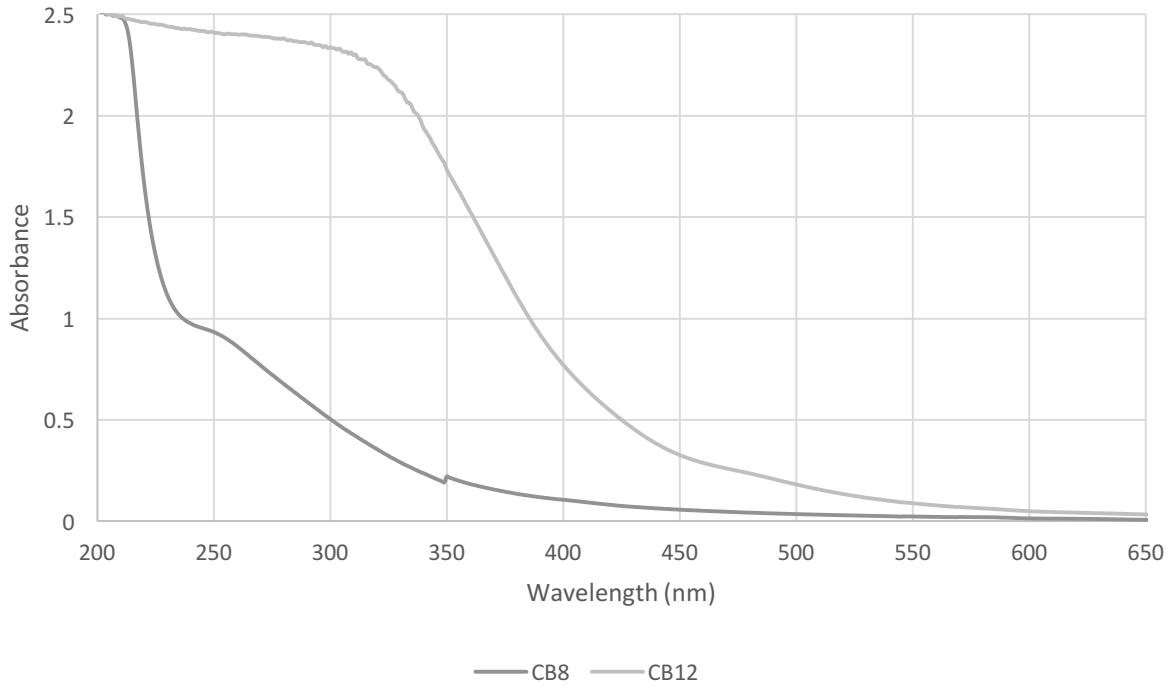

Figure 2-1 UV/visible spectrum of CB08 and CB12 films with air as blank, transmission mode

2.3.2 Stress/Strain

Tensile tests of CB08 and CB12 were performed with a Shimadzu brand strength tester, while samples were both dry and wet. The wet tests were performed to demonstrate the change in structural properties of chitosan bioplastic immediately after soaking in water. For the wet tests, samples were soaked in water for 1 h immediately prior to testing.

To prepare all the samples, 1 x 2.1 cm strips of bioplastic were cut from the films with a laser cutter. The strips were uniformly notched to ensure breakage in the middle. They were then all soaked in 0.5 M NaOH for 6 to 8 hours, allowed to dry, rinsed in water for 6 to 8 hours, then dried again. The soaking was done after cutting, because the soaking causes some warping. Warping was further reduced by pressing strips while drying.

For the strips tested while dry, paper grips were attached with strong glue and tape at each end, so that the stretching machine could hold on without slipping. The soaked samples needed waterproof grips, so those were fashioned from medical self-adherent elastic wrap.

Bioplastic shrinks during the NaOH soaking process, and the samples did not all shrink uniformly. Therefore, care was taken to measure the width of the notched area, thickness of film at the notch, and gauge length (distance between the two grips) before each test. These measurements are entered into the Trapezium X software, which takes them into account when calculating stress and strain data. Strips were stretched at a speed of 5 mm/min. Forty-nine strips of dry CB12, 35 strips of dry CB08, and 73 strips of wet CB08 were tested. See results in Table 2-1. Examples of typical curves are shown in Figures 2-2 and 2-3. Max slope data was determined by using the Trapezium software to manually overlay a line onto the graph of each test, at the place where the slope appears highest (though not including very small occurrences of high slope due to experimental noise). As seen in Figure 2-3, not all of the graphs display the force returning to zero

at the end of a test. This is because a short time after the material breaks, the machine stops measuring force.

When wet, the CB12 became too fragile to handle, so results were not obtained for it. However, the CB08 performed well. Understandably, it lost some strength when wet, but was able to stretch about 30% before breaking.

Table 2-1 Stress/strain characteristics of chitosan bioplastics

	Tensile Strength (N/mm^2)	Maximum Strain (%)	Maximum Slope (N/mm^2)	n
CB12 (Dry)	47 ± 25	3.6 ± 2.1	2500 ± 1600	49
CB08 (Dry)	93 ± 35	7.5 ± 2.7	2800 ± 1600	35
CB08 (Wet)	6.9 ± 7.1	31 ± 8.7	41 ± 69	73

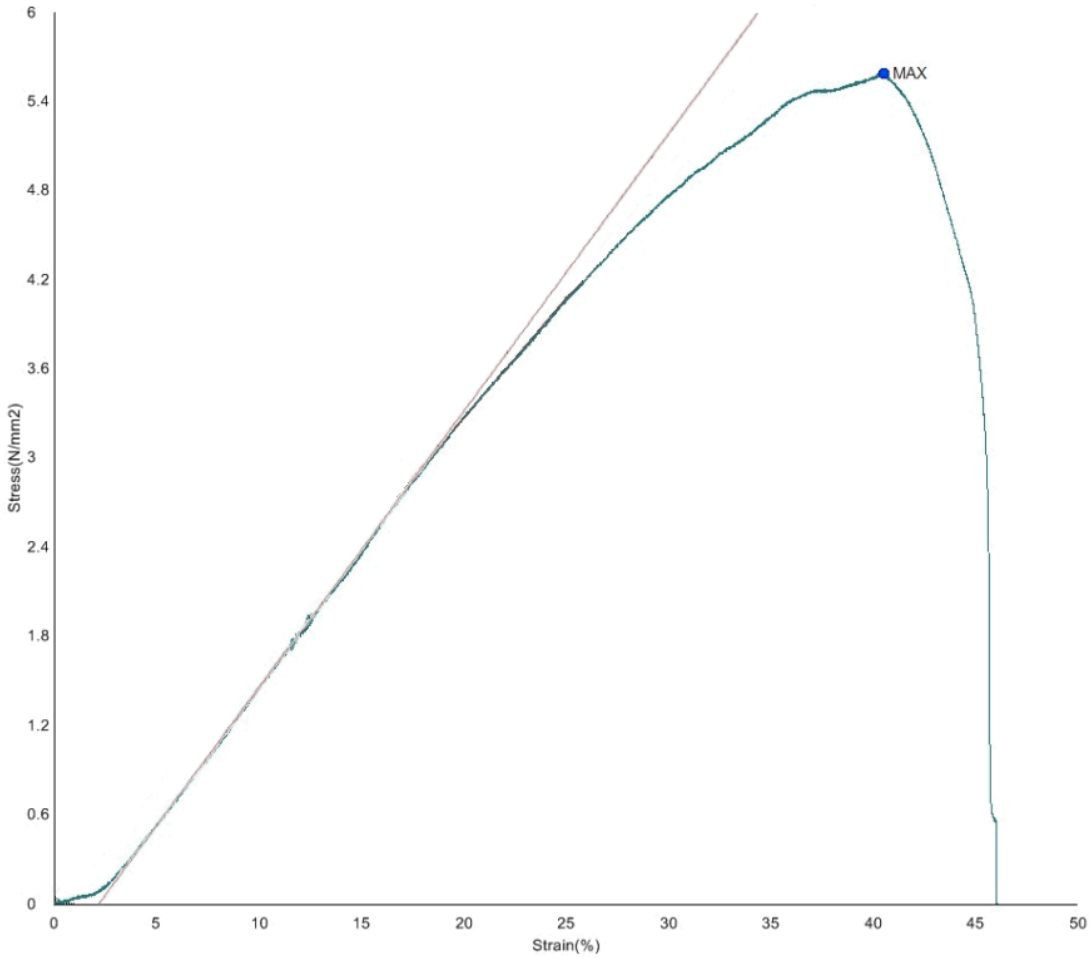

Figure 2-2 Stress/strain curve for typical CB08Wet sample as presented by TrapeziumX software. The straight line overlay is used to determine the maximum slope.

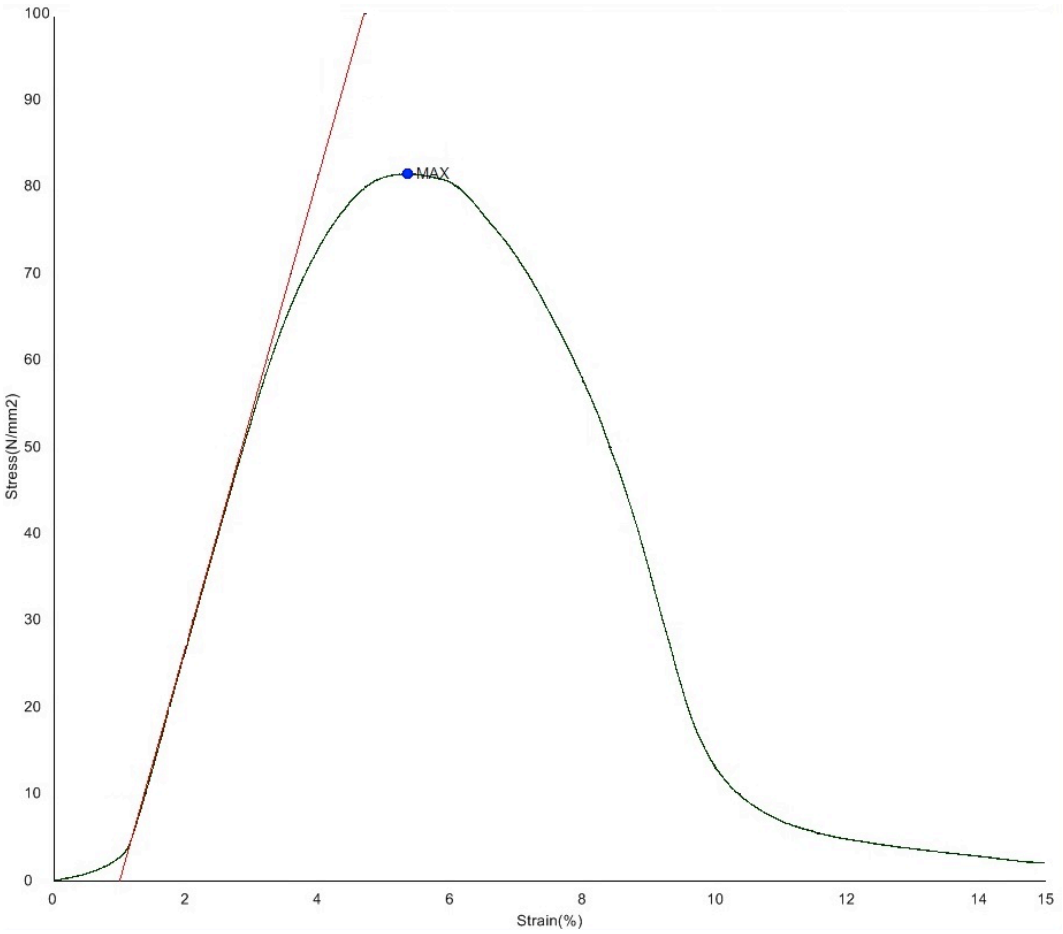

Figure 2-3 Stress/strain curve for typical CB08 dry sample as presented by TrapeziumX software. The straight line overlay is used to determine the maximum slope.

In comparison with similar experimental materials, Tan et al.[23] created a composite polyethylene/chitosan film with tensile strength between 7.5 ± 0.6 and 10.1 ± 0.3 N/mm^2. This resembles our pure chitosan bioplastic when wet, and is much weaker than the dry CB. Their maximum strain ranged from around 7 to 20%, depending on ratio of components, comparable to CB. The Young's Modulus for the polyethylene/chitosan was between 200 and 250 N/mm^2, which is much lower than for the dry CB.

Ifuku et al. (2009) created surface-deacetylated chitin nanofiber reinforced chitosan films.[27] The Young's Modulus of the films ranged between 2000 to 9000 N/mm^2 , depending on

nanofiber content, while the tensile strength ranged from 40 to 160 N/mm^2 . The CB in the present study is comparable with the weakest specimens from Ifuku et al.

2.3.3 Swelling

Ten 10x10 mm^2 squares each of CB08 and CB12 were soaked for 8 hours at 25 °C (approximate room temperature) and in a 37 °C (approximate body temperature) incubator. It was found that CB12 is more prone to swelling than CB08, and the incubated samples swelled slightly more than room temperature samples (Table 2-2). CB08 did not swell when soaked at 25 °C.

Unfortunately, no other paper describing similar chitin-based materials has reported any quantitative data on swelling. However, it should be an important point of comparison between different formulations, because swelling and water stability are essential to understand when considering practical applications.

Table 2-2 Average side length of CB squares after soaking 8 hours, some samples at 25 °C and some at 37 °C (starting size 10 x 10 mm^2)

Temperature:	25 °C	37 °C
CB08	10 ± 0.0 mm	10.7 ± 0.7 mm
CB12	10.2 ± 0.4 mm	12.7 ± 0.7 mm

2.3.4 Scanning Electron Microscopy (SEM)

After fracturing sample CB08 with the Shimadzu strength tester, the sample was examined by SEM. It was found that the films dry with horizontal layers, estimated to be about 30 nm thick (Figure 2-4).

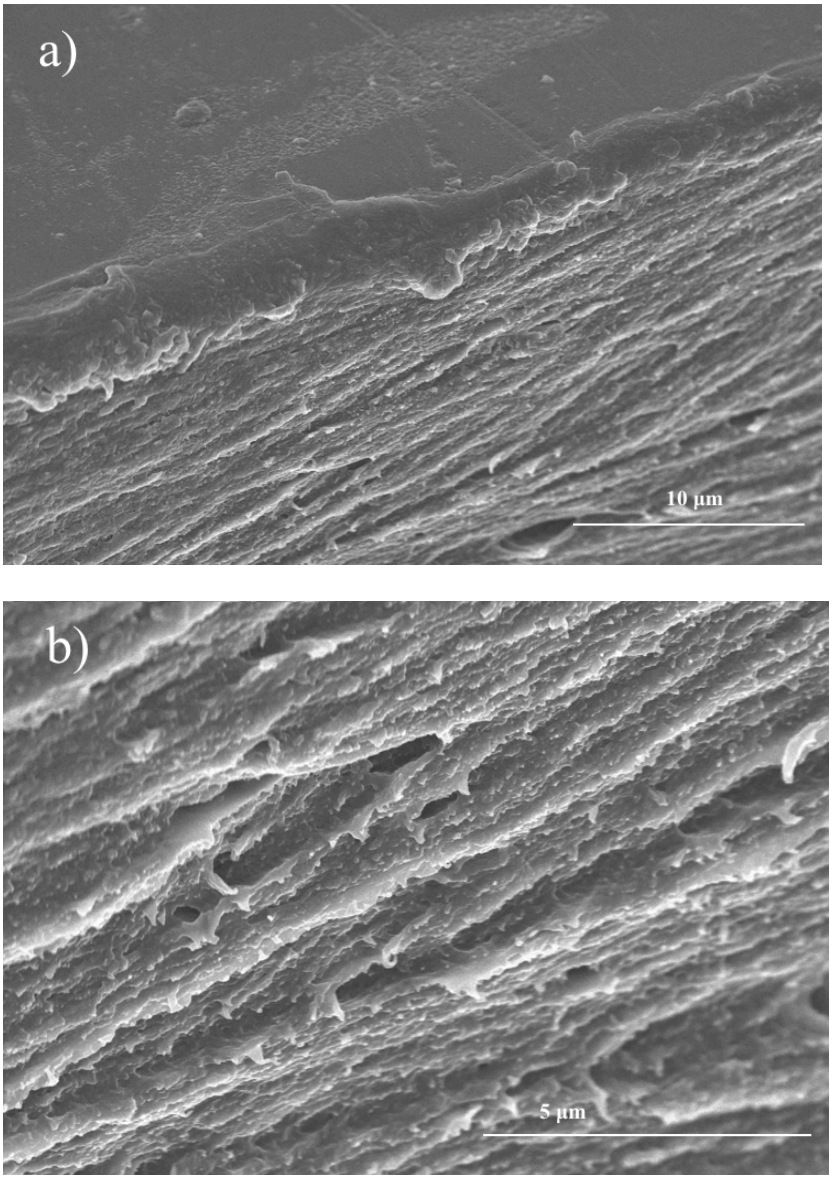

Figure 2-4 Scanning Electron Microscopy (SEM) images of chitosan bioplastic edge after fracture, at two different magnifications.

2.3.5 Thermogravimetric Analysis (TGA)

Thermogravimetric analysis (TGA) shows how the films decompose in air as the temperature is gradually increased from 25 °C to 750 °C at 5 °C/min intervals (Figure 2-5). Samples were lyophilized before testing, and the remaining water evaporated as the temperature reached 100 °C. The inflection for the first stage of thermal decomposition was around 350 °C in both samples, where weak bonds are broken. In the second stage, some remaining covalent bonds were broken as the specimens turned to ash.

The inflection point occurs near 350 °C in all 4 tests, which will be used to distinguish the two stages of thermal decomposition. The CB08 retained 46% of its mass at 350 °C in both tests. The CB12 retained 54% of its mass at 350 °C in the first test, and 47% in the second test. The CB08 and CB12 thus appear similar in this regard, indicating that the weak bonding of the materials is similar.

During the 2nd stage, the CB12 finished degrading at a lower temperature than CB08 (~600 °C as compared to ~700 °C), likely because the molecules were weakened by the longer deacetylation time. It is unclear whether this difference is due to variations in deacetylation because the EA results for deacetylation were inconclusive (section 2.3.6).

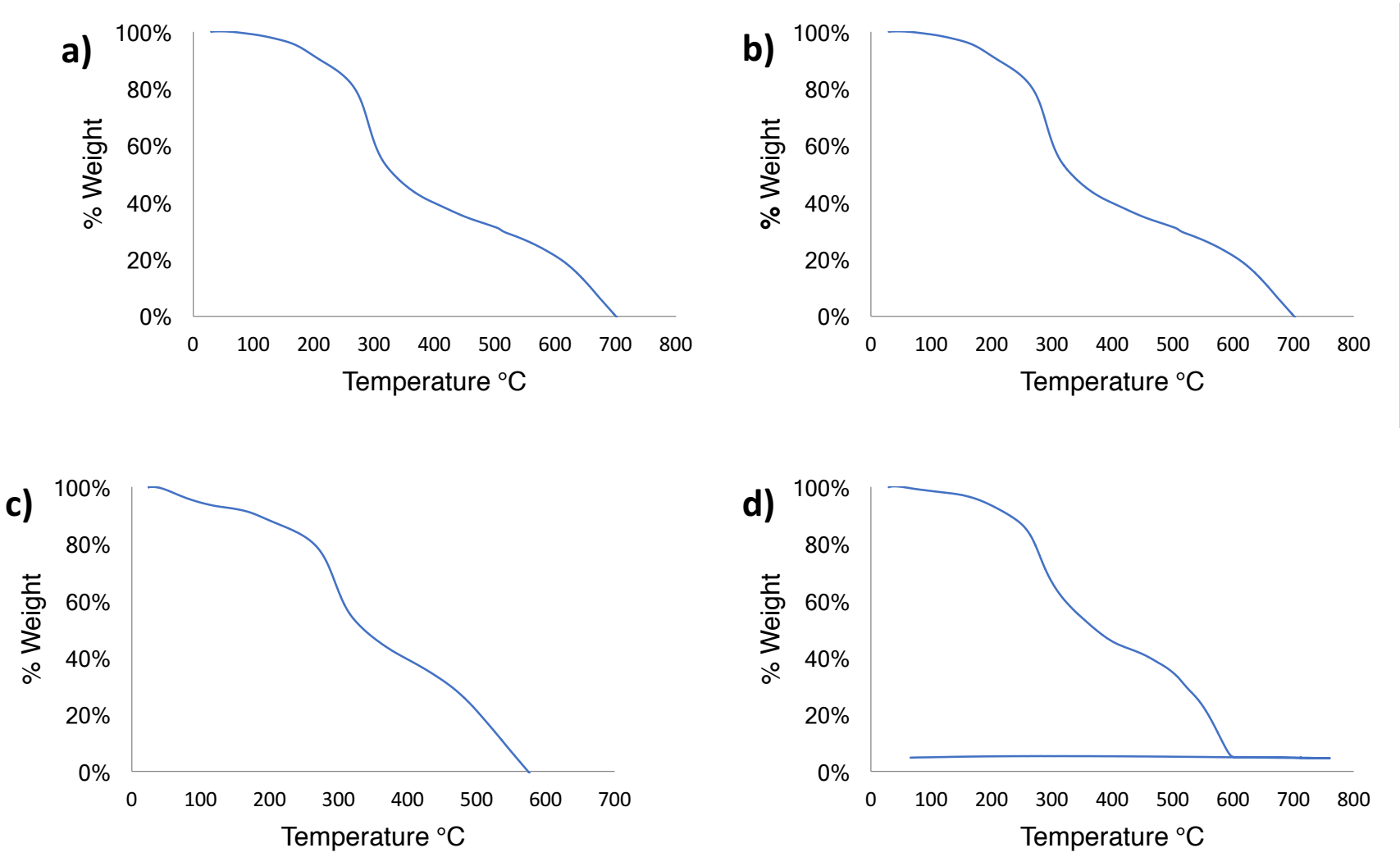

Figure 2-5 Duplicate TGA runs for CB08 and CB12, a) CB08 #1; b) CB08 #2; c) CB12 #1; d) CB12 #2. Samples were heated at 5 °C/min under air.

2.3.6 Elemental Analysis (EA)

Because deacetylation affects the relative amount of nitrogen in chitin/chitosan, elemental analysis can be used to determine the degree of acetylation in a sample.[23] As chitosan is missing an acetyl group (Figure 1-1), the mass percent of N should be higher in chitosan than chitin. Samples of CB08 and CB12 (pre-NaOH treatment, to avoid presence of water) were dried by lyophilizing overnight, then stored in an air-tight container before EA analysis. Contrary to expectation, the N content decreased with increasing deacetylation time. This indicates a problem with the method, or perhaps contamination.

The amine on chitosan is a strong base, one possibility is that these samples resorbed water after removal from the lyophilizer. In Table 2-3, the theoretical result is calculated for chitosan with one H_2O absorbed per monomer. These numbers reflect the experimental values with respect to the change in C and H percent. However they don't explain the lower than expected N% in all experimental samples, with little variation between the chitin and chitosan.

Table 2-3 EA results for purified crab chitin, CB08, and CB12, compared with theoretical values for the pure substances. Oxygen percentages were omitted because they cannot be detected by EA.

		N%	C%	H%
Theoretical values	chitin	6.90	47.32	6.40
	chitosan	8.69	44.75	6.83
	chitosan + water	8.38	35.93	7.78
Experimental values	chitin	6.36	42.49	6.49
	CB08 chitosan	6.11	38.97	7.47
	CB12 chitosan	5.75	37.44	6.96

2.3.7 Fourier-Transform Infrared (FTIR) Spectroscopy

The CB08 and CB12 shared similar peaks at 1636 cm^{-1}, 1152 cm^{-1} and 659 cm^{-1} (Figure 2-6). Smaller peaks shared by each sample were observed at 1540 cm^{-1}, 1406 cm^{-1}, 1066 cm^{-1}, and 1021 cm^{-1}. Chitosan has two different O-H groups which contribute to the broad signal around 3000 - 3500 cm^{-1}. Additionally, the secondary amines contribute to the signal in the range above 3000 cm^{-1}. Typical bending and stretching frequencies for the functional groups found in chitin and chitosan are detailed in Table 2-4.

Other papers studying deacetylated chitin via FTIR spectroscopy describe a number of different spectral bands. Tan et al. studied a chitosan/synthetic polymer blend and discussed amide I and amide II bands at 1650 cm^{-1} and 1658 cm^{-1}. They state that the strength of the band at 1658 cm^{-1} represents acetyl groups. CB08 and CB12 samples do have a small peak near these values, at 1636 cm^{-1}. Tan et al. mention a C-O stretching band at 1030 cm^{-1}, which is mirrored by CB samples at 1021 cm^{-1}.

Ifuku et al. (2013) describe two major bands at 1231 cm^{-1} and 1748 cm^{-1} corresponding to the acetyl group. The absence of these bands in CB suggests a high degree of deacetylation.[20]

Nair & Dufresne measured residual proteins using the peak at 1540 cm^{-1}. CB has a significant peak at 1540 cm^{-1}, indicating residual proteins.[29]

Wu described bands at 2900 cm^{-1} and 3000 cm^{-1} for N-H stretching, 1650 cm^{-1} for C=O stretching, and 1557 cm^{-1} for NH vibration.[30] They also noted that the ratio of bands at 1379 cm^{-1} and 2900 cm^{-1} has been suggested for use as a crystallinity index for chitin/chitosan. However, neither of those peaks showed up in CB.

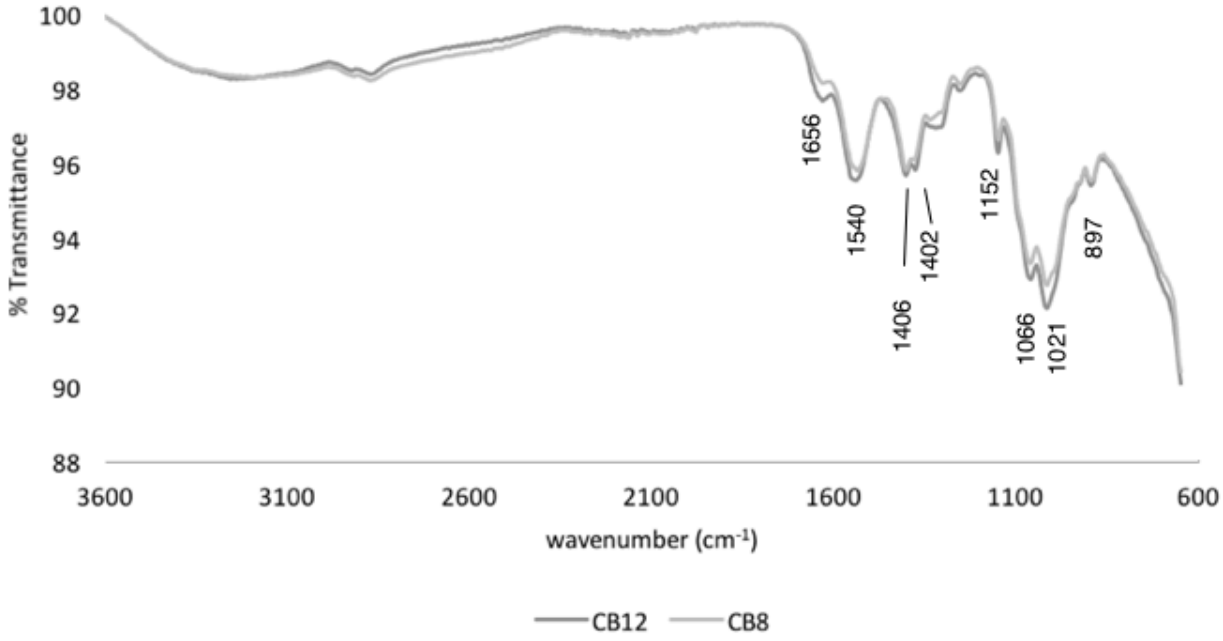

Figure 2-6 FTIR spectra of CB08 and CB12.

Table 2-4 Typical bending and stretching frequencies for bonds found in the listed functional groups, all of which can be found in chitin and/or chitosan.[31]

Functional Group	Vibration Type	Characteristic Absorptions (cm^{-1})	Intensity
Alcohol			
O-H, H-bonded	Stretch	3200-3600	Strong, broad
O-H, free	Stretch	3500-3700	Strong, sharp
C-O	Stretch	1050-1150	strong
Alkane			
-C-H	Bend	1350-1480	strong
Amine			
N-H	Stretch	3300-3500	medium
C-N	Stretch	1080-1360	strong
N-H	Bend	1600	medium
Carbonyl			
C=O	Stretch	1670-1820	strong
O-H	Stretch	2500-3300	
Amide			
C=O	Stretch	1640-1690	strong
N-H	Stretch	3100-3500	medium
N-H	Bend	1550-1640	
Ketone			
acyclic	Stretch	1705-1725	strong
Ether			
C-O	Stretch	1000-1300	strong

2.3.8 X-Ray Diffraction (XRD)

X-ray diffraction was used to study the crystallinity of CB08 and CB12 before and after strengthening with NaOH (Figure 2-7). The wide peak shapes are characteristic of a nanocrystalline polymer, crystalline regions surrounded by amorphous tangles. Surprisingly, the XRD profiles for each of the four samples are markedly different. Attempts to model the results with peak-fitting software were inconclusive. Percent crystallinity calculations were statistically inconclusive and difficult to compare between scans because the peak shapes are so different. Each

sample underwent definitive change in crystallinity after the NaOH treatment, and CB12 saw an increase at 19.8°, which is a peak characteristic of chitosan.[18] Given that the FTIR data also showed neither of the peaks used to measure crystallinity of chitin, it is likely that CB has quite low crystallinity overall.

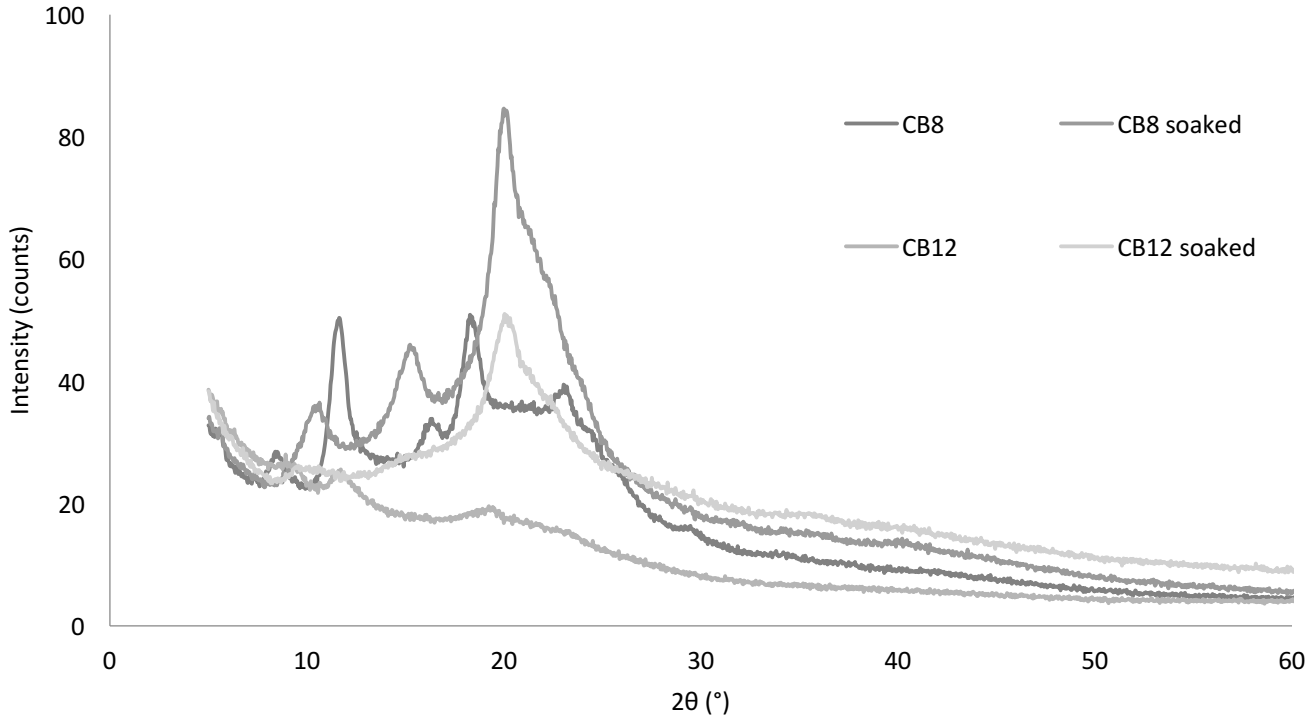

Figure 2-7 XRD patterns of CB08 and CB12 before and after soaking in water.

2.3.9 Contact Angle

By measuring the contact angle of a drop of water on a surface, the affinity of the surface to water can be evaluated. Contact angle was measured by photographing a drop of water on the surface of CB08 and CB12, and mathematically analyzing the angle using computer software

(Figure 2-8). As the contact angle is less than 90°, the material is considered slightly hydrophilic (Table 2-5). There is one other mention in the literature of contact angle measurements on a chitosan surface. Farris et al. conducted contact angle measurements on a number of biopolymer-based coatings, comparing gelatin, pectin, pullulan, and chitosan materials.[32] To create the chitosan coating, they purchased shellfish chitosan with an 85% degree of deacetylation and a molecular weight ranging from 50 000 to 60 000 Da. They then dissolved it in 5 wt % hydrochloric acid to create a gel, which was then used for coating deposition. The method is similar to the one used in this thesis, but their coatings were much thinner than films described in this thesis. Among the coatings they tested, chitosan was the most hydrophobic, with a water droplet contact angle of 98° ± 2°. The contact angle measurements for chitosan films in this project are somewhat lower.

Table 2-5 Contact angle data for CB08 and CB12, n = number of samples measured

	Contact Angle °	n
CB08	80 ± 4	4
CB12	80 ± 2	6

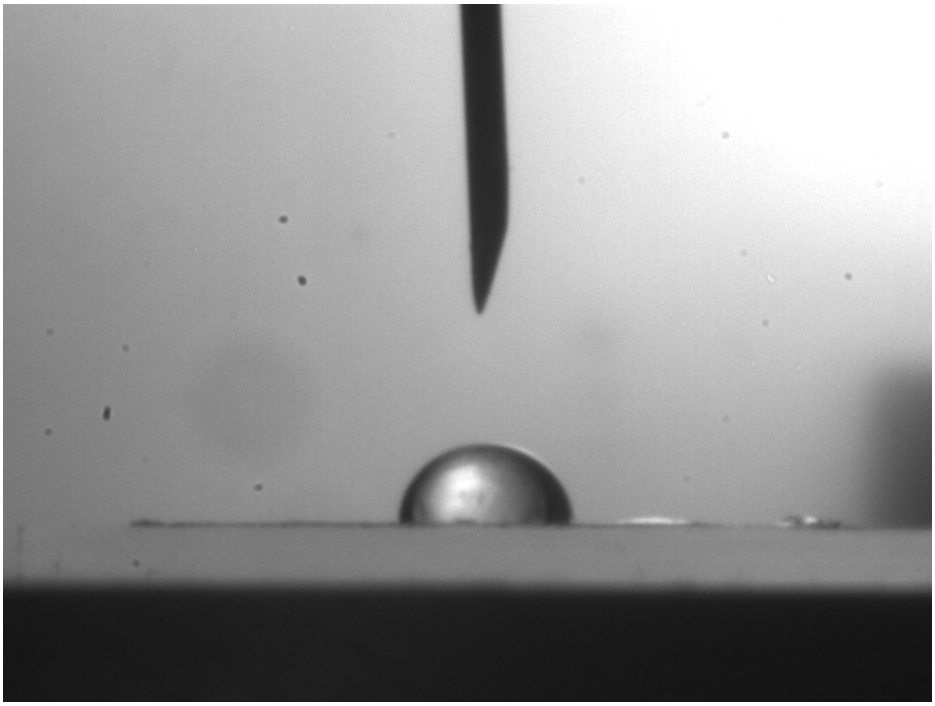

Figure 2-8 Example photograph used for contact angle measurement

2.4 Discussion and Future Work

The CB has good potential for commercial use, after additional R&D. The data provided here will be of use to those who wish to work further with this material and make comparisons between different fabrication methods. In particular, the CB08 had preferable characteristics in comparison with CB12. CB12 appears to be "overcooked" due to the longer deacetylation time: the slightly orange color, weaker physical strength, and faster decomposition during TGA support this conclusion. In addition to better performance during strength testing, the CB08 swelled less than CB12 when soaked in water at 25 °C and 37 °C, showing that it is more stable in wet environments at room temperature and body temperature. Now that it is known that 8 hours of deacetylation is preferable to 12, further experiments could be conducted to optimize the deacetylation time, for example, comparing 7.5, 8, and 8.5 hours.

To develop CB further, research should be done to investigate how it may be shaped or molded. The fabrication process used here, of letting a liquid solution dry in a dish over a period of weeks, doesn't lend itself well to complex shapes. Perhaps the solution could be cast into some kind of mold, and the moisture could be wicked away through a membrane. CB may have heat-ductility like some other plastics, suggesting an investigation into whether it can be re-shaped when warm. Or a combination of all these methods – dry the solution into a gel, heat it so that it flows into a mold, and then dry further. Fastening glue could also be explored two or more flat rectangles of CB could be glued together to create a plastic bag, or packaging around an item. The flexibility of the material could even lend itself to use as an alternative to current petro-chemical based "blister-packs".

With a viable product in hand, more research would still be needed in order to optimize the fabrication process, in particular, working to cut down excessive use of NaOH and HCl, seeking a solution both financially viable and environmentally friendly.

Chapter 3 – Introduction to Polypyrrole and CNCs

3.1 Polypyrrole Background

Polypyrrole (PPy, Figure 3-1) is a synthetic organic conductive polymer. Like all conductive polymers, the electrical conductivity arises from the alternating carbon-carbon double bonds. Polypyrrole is interesting for a myriad of technological applications, from batteries to supercapacitors to electronic biocompatible implants.

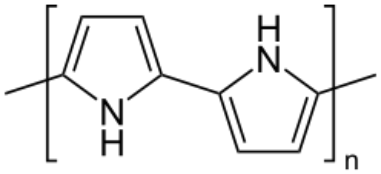

Figure 3-1 Polypyrrole

In order to conduct electricity, synthetic conductive polymers must be activated through oxidation (most commonly) or reduction. Polypyrrole can be easily oxidized and reduced by the application of current. P-doping by oxidation is illustrated in Figure 3-2. The counterion A^- diffuses in and out the polymer. The movement of the counterion can cause significant change in volume. This can be useful in the case of some PPy-based actuators, but can also damage the polymer matrix.[33]

The oxidized pyrrole monomers have a different energy than the others, and cause a deformation in the polymer. The combination of this deformation and corresponding electron/hole pair is known as a polaron. When enough polarons are present, they combine to form bipolarons, which are more energetically stable. When current is applied to the polypyrrole, the movement of bipolarons along the backbone is the basis for bulk flow of electrons.[33]

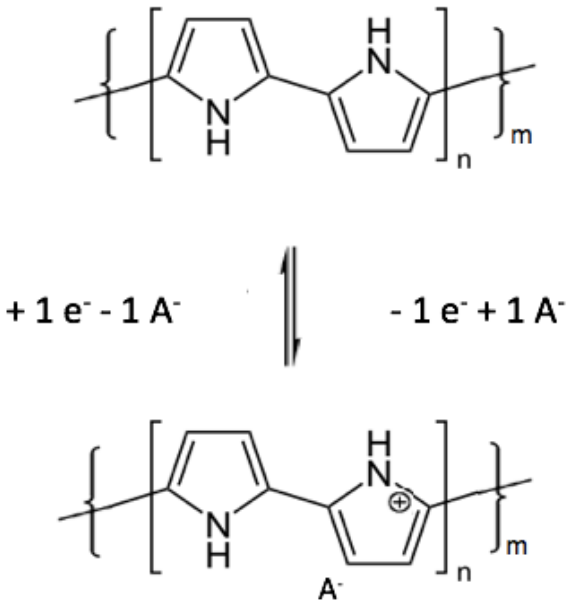

Figure 3-2 Polypyrrole doping scheme. A^- is the anion, n indicates degree of doping, m indicates molecular weight.

Conducting polymers are useful because they can be used to transmit electrical signals without using metal or silicon. Many conducting polymers are flexible and can be incorporated into other materials such as non-conducing plastic polymers. Polypyrrole is particularly interesting to work with because it is organic, biocompatible, and easy to synthesize.

As an isolated substance, polypyrrole is a powder. To give it form, it must be intercalated with something else. For example, Wang et al.[34] made flexible polypyrrole composite films by mixing PPy with the cathode $LiFePO_4$, for use in a rechargeable battery. Ilicheva et al[35] mixed polypyrrole with hydrophilized polyethylene to create strong elastic conductive films.

Polypyrrole must be associated with a dopant to conduct electricity. It can be synthesized with oxidants such as $FeCl_3$ or $(NH_4)_2S_2O_8$. As a result of the reaction, anions from the oxidants become incorporated as dopants (Cl- from $FeCl_3$ or HSO_4^-/SO_4^{2-} from $(NH_4)_2S_2O_8$). The other way

to polymerize PPy is through the electrochemical approach, and the dopant anions are captured from the electrolyte solution. PPy is soluble in both aqueous and organic solutions, so many types of dopants have been used for this electrochemical method, including catalysts, complexing agents, and biomolecules.[36]

3.2 CNC Background

In this study, polypyrrole was combined with chiral cellulose nanocrystals (CNCs) as a scaffold material. The aim was to create a PPy film in which the PPy is affected by the chiral nematic arrangement of the chiral cellulose scaffold, resulting in interesting electronic or optical properties.

CNCs have been studied and developed extensively by the MacLachlan group – this study contributes to that body of work. Cellulosic material can be hydrolyzed with sulfuric acid to yield cellulose crystallites, which assume a chiral nematic formation when suspended in water.[37] When a CNC solution is allowed to dry by evaporation, the solid film of crystallites retains the chiral nematic formation (Figure 3-3).

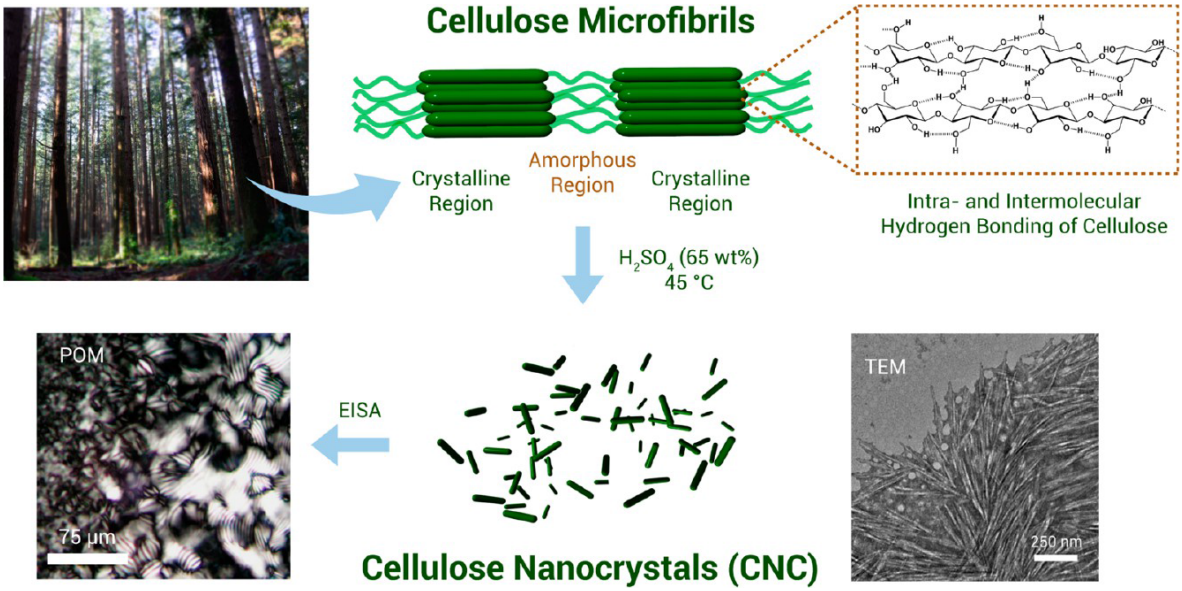

Figure 3-3 Cellulose nanocrystals for this project are derived from wood, through acid hydrolysis. The nanocrystals are found in cellulose microfibrils, which have regions where the cellulose alternates between crystalline and amorphous regions. Cellulose is held together through hydrogen bonding. During evaporation-induced self-assembly (EISA), the fingerprint texture of the liquid crystal can be viewed by polarized optical microscopy (POM). Spindle shape of the nanocrystals are revealed by transmission electron microscopy (TEM). Image from Kelly et al.[38]

CNCs have three different levels of chirality. The individual glucose monomers are chiral, and the glucose polymers collectively form chiral crystallites. When the CNCs are dried from solution, they form a film of layers upon layers. Each horizontal layer is made of crystallites oriented in a particular direction. At each successive layer, the axis of orientation is shifted slightly clockwise, creating an overall left-handed chiral twist in the layers of the film.

Variations of the solvent (such as pH) and the presence of other molecules in the solution can affect the pitch of the dried CNCs. The pitch refers to the distance within which the film's layers make one complete 360° twist (Figure 3-6). Because the pitch of CNCs is on the size order of the wavelengths of visible light, the structure diffracts light, creating iridescence. The colors of pure CNC films, ranging across the visual spectrum, arise solely from its structure. Bragg's law, 2

d sin θ = n λ, governs the colors that are scattered, and is described in Figure 3-4. When light shines on CNC, some photons pass through it while others are reflected by the cellulose crystallites. When light waves reflect off of different horizontal layers within the film, they are occasionally in phase with each other, and this constructive interference results in structural color. The observed color is determined by the wavelength of light that is reflected from the film. When viewing the film from different angles, or changing the angle of incidence of light, different colors can be seen resulting from different constructive interference patterns (Figure 3-5).

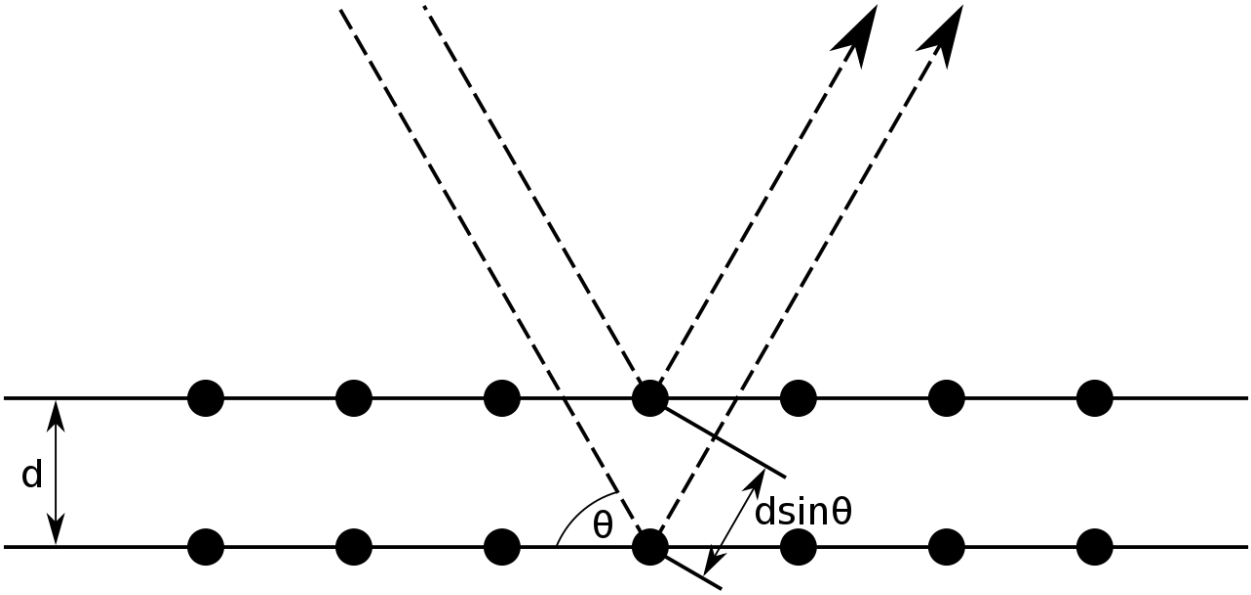

Figure 3-4 Bragg's Law: 2 d sin θ = n λ, where n is a positive integer. Incident light at angle θ (dotted lines) is reflected by two different crystal planes. Spacing between planes is d. Image from Wikimedia Commons.

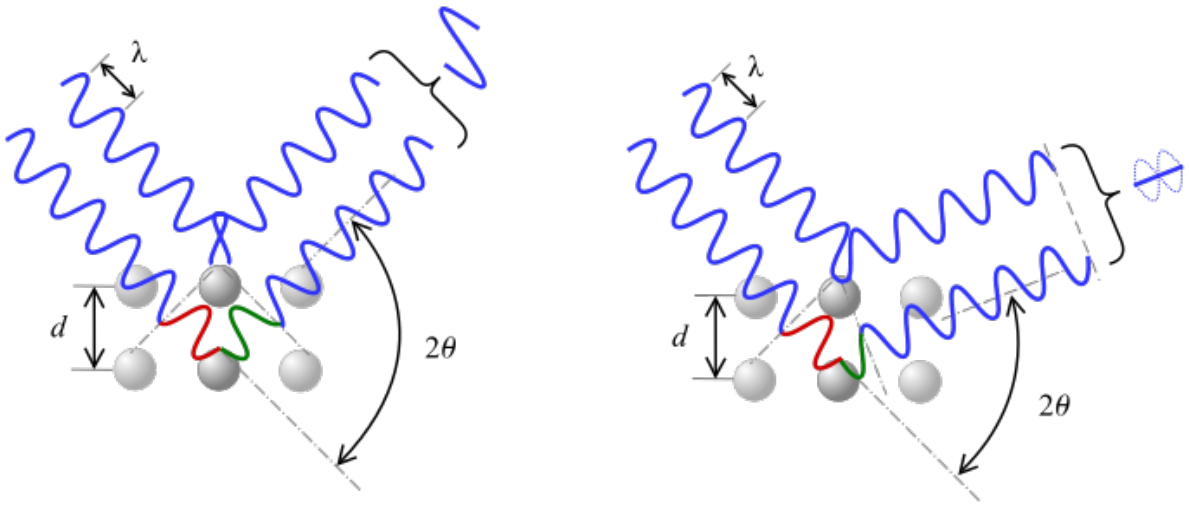

Figure 3-5 a) Destructive interference. b) Constructive interference of light waves reflected from two crystal planes according to Bragg's Law (Figure 3-4). Image from Wikipedia Commons.

CNCs always dry in a pattern with a left-handed helical twist; the reason for this arrangement is not yet fully understood. This helical structure influences the nature of reflected light: light reflected off of the films contains only left-handed circularly polarized waveforms. Circular dichroism (CD) spectroscopy is used to characterize this polarization handedness across the spectrum of light.

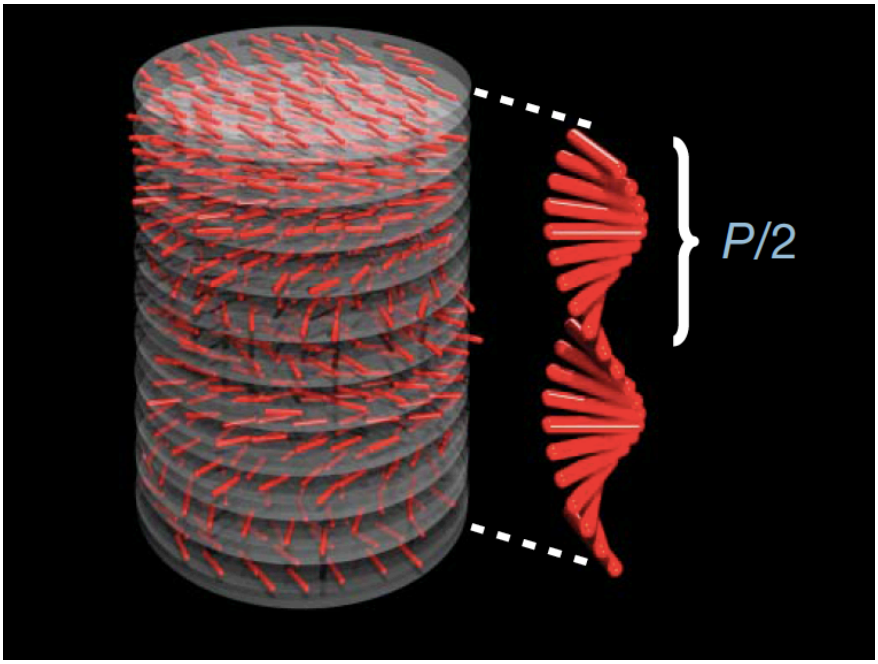

Figure 3-6 The pitch of CNCs is illustrated. Each layer is rotated slightly with respect to the last, resulting in a twist of the medium. The length of the pitch refers to one 360° twist. Image is from Shopsowitz et al. (2010).[39]

3.3 Chiral Conducting Polymers

In their review of chiral conducting polymers in 2009, Kane-Maguire & Wallace point out that helical chirality plays a vital role in many biological polymers, and is therefore a topic well worth exploring with synthetic polymers. [36] Already, applications have been found for chiral sensors, catalysts, and chromatographic separation column coatings. Application frontiers include electrochemical chiral sensing and electrochemical asymmetric synthesis.

Kane-Maguire & Wallace describe 3 strategies to create chiral conductive polymers:

1) Polymerize the conductive polymer in the presence of an enantiomerically pure substituent.

2) Add a chiral dopant anion to the polymer chain (demonstrated for the conductive polymer polyaniline).

3) Twist the polymer chain within its matrix. However, twisting of the polymer is not ideal as it lowers conjugation and conductivity.

The incorporation of PPy into the chiral nematic structure of CNCs represents a new fourth category: Incorporate the conductive polymer into a nanostructured chiral matrix (no twisting involved). The PPy was not mixed with CNCs until after it was polymerized, so the chiral structure was not intended to have any direct impact on the polymer chain conformation.

The work described in this thesis represents the second attempt by the MacLachlan group to create a chirally-structured organic conductive polymer. First, in 2013, Mehr et al. templated poly(p-phenylenevinylene) (PPV) in chiral mesoporous silica.[40] The silica mold was created by drying a film from a mixture of CNCs and $Si(OMe)_4$. The CNCs cause the solution to dry in a chiral nematic pattern, while the tetramethyl orthosilicate undergoes hydrolysis and condensation as the solvent evaporates, leaving behind silica. The CNC/silica composite has a high surface-area with a pore diameter of ~3-10 nm. The cellulose is then removed by acid-catalyzed hydrolysis to leave behind highly porous and chiral silica films. The pores themselves follow the chiral pattern, interacting with light for a bright iridescence.

PPV had previously been encapsulated in mesoporous silica, but this was the first time it was included inside chiral porous silica. PPy was polymerized in-situ by first activating the surface hydroxyl groups of the silica with a methanolic solution of tetrabutylammonium hydroxide, which then allows the polymerization of xylene bis(tetrahydrothiophenium bromide) to PPV. Mehr et al. confirmed with circular dichroism (CD) spectroscopy that the PPV did assume a left-handed helical structure within the host, evidenced by the negative signal CD for PPV at 430 nm. It is unknown whether this chirally-organized conducting polymer had any unexpected (or expected) electrical or chemical effects, as no testing of such properties was reported.

3.4 Cellulose Polypyrrole Composites

Some other groups have successfully created composites of polypyrrole with other cellulosic materials. Nystrom et al. were able to successfully coat wood-derived nanocellulose fibers with PPy to create an electrically conductive composite.[41] Microfibrillated cellulose, in hydrogel form, was mixed with pyrrole precursor, then $FeCl_3$ oxidant. In this way, the polypyrrole fibers were attached to the cellulose fibers immediately upon conception. The mixture was then filtered to collect solids which were dried to a film.

Liew et al. used an electrochemical deposition approach.[42] Using a glassy carbon electrode surface, they deposited PPy onto cellulose nanocrystals, thereby incorporating the negatively-charged nanocrystals into the polymeric structure as counterions. Using cyclic voltammetry and electrical impedance spectroscopy, they showed that polypyrrole templated in this way had comparable electrical properties to that of similar composites made with carbon nanotubes. Cellulose nanocrystals are much cheaper than carbon nanotubes, which shows why the combination of polypyrrole and cellulosic materials is a promising field to study.

Composites of PPy with nanofibrillar cellulose, carboxymethylcellulose, and xylan were compared by Sasso et al.[43] The PPy was chemically synthesized in the presence of each cellulosic material. The nanofibrillar cellulose composites had the highest conductance, albeit the weakest mechanical properties.

3.5 Goal of this Thesis (CNC/PPy Project)

The goal of this project was to attempt templating polypyrrole onto chiral nematic cellulose as a scaffold, and study any resulting electronic properties.

Chapter 4 – Composites of Chiral Nanocrystalline Cellulose and Polypyrrole

4.1 Sample Preparation

4.1.1 Film Preparation

Pyrrole monomer is a clear liquid that degrades in the bottle when kept at room temperature. Before use, the pyrrole was distilled and stored in a -80 °C freezer. All glassware for the reaction was washed with hexane, acetone, then methanol. The round-bottom reaction flask was submerged in an ice bath with a magnetic stir bar, and the inside rinsed with deionized water to prevent polymer sticking to the surface of the glass. The beaker was covered with foil to prevent light damage. 0.560 g (2.45 mmol) of the oxidant, ammonium peroxydisulfate, was chilled and mixed into 25 mL chilled deionized water. With 1.743 g (25.98 mmol) of pyrrole in the beaker, the oxidant solution was added dropwise, yielding immediate precipitation of black polypyrrole. When pyrrole is oxidized, each monomer forms a radical cation species. Two such radicals join together to form a dimer, eliminating hydrogen. This process continues until a long chain is formed (Figure 4-1). The reaction is rapid, but it was allowed to proceed for 20 minutes before filtration. All the mixing was done in an ice bath cooled flask so the reaction would proceed slowly, resulting in longer chains of polymer rather than a greater number of shorter chains. The reaction was kept on ice and allowed to proceed before quenching with 50 mL methanol.

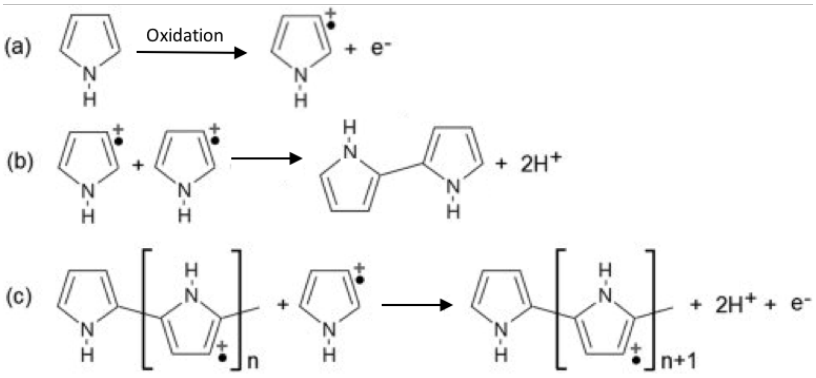

Figure 4-1 Oxidative polymerization of pyrrole

To remove the excess reactants, the mixture was centrifuged, and the PPy pellet repeatedly rinsed with methanol and re-centrifuged until the supernatant was clear. The vial of PPy in methanol was wrapped in aluminum foil and stored in the refrigerator to prevent damage from light and heat.

Before mixing with liquid CNCs, the PPy was sonicated to suspend it in the methanol. The CNC suspension was produced by FPInnovations, with 4 wt% CNCs, pH 6.4, and conductivity of = 395 μS/cm. When left to dry, it formed chiral nematic films. To mix CNCs and PPy suspension, they were pipetted into vials together then sonicated. Seven mixtures were made, each using around 8 g of CNC solution and variable amounts of PPy. Blank samples were made from pure CNC and pure PPy suspension (Table 4-1).

4.1.2 Experimental Details

All chemicals were purchased from Sigma Aldrich or Alfa Aesar and used as received. A Hitachi S-4700 Field Emission SEM was used to collect electron microscopy images. The X-ray diffractometer was a Bruker D8-Advance with Bragg Brentano configuration, copper $K\alpha_1$ & $K\alpha_2$ radiation source, nickel filters, LynxEye detector, and slits 1 mm divergent, 8 mm anti-scatter, 2.5°

soller. Two potentiostats were used; one a Bipotentionstat Model AFCBP1, from the Pine Instrument Company with AfterMath software, and the other an Autolab Potentiostat Galvanostat, model PGSTAT12. A Thermolyne 1400 benchtop furnace was used to heat the bombs.

4.2 Results

4.2.1 Physical Characteristics

The PPy content in the dried films was calculated by comparing the weight of the dried film to the expected weight contribution of the CNC in the film. The "blank" film was created with only CNCs: 8.009 g of CNC solution yielded 0.180 g of dried material. That information was used to estimate the mass of dried CNC in each film, based on the grams of CNC solution used for that film. Any remaining mass in the dried film was assumed to have come from PPy. The weight percent of PPy in the films was calculated from this data.

When dried, several samples cracked but most did not. The PPy appeared to be evenly distributed throughout the CNCs, with no clumping or spotting. When the CNCs were overloaded with PPy, the sample dried with a layer of black PPy underneath the composite layer. However, in this batch, no samples were overloaded, so the highest loaded sample CNC/PPy-6 was selected for further testing.

The PPy blank dried as a powder (Figure 4-2). The CNC blank dries as an iridescent translucent film (Figure 4-3). When viewed through left- and right-handed circularly polarized lenses, it is seen to reflect only the left-handed circularly polarized light. The dry film of CNC/PPy-6 looks similar to the CNC blank, but with darker color (Figure 4-4). It has similar circular polarizing characteristics, indicating that some chiral nematic form is present. Figure 4-5 demonstrates that the films are flexible enough to bend with the fingers.

Table 4-1 CNC/PPy film preparation details

Sample Name	mL PPy	g CNC solution	Dry Film (g)	Calculated solid PPy in dry film
CNC-Blank	0.0	8.009	0.180	0.0%
CNC/PPy-0.5	0.5	8.009	0.182	1.0%
CNC/PPy-1	1.0	7.992	0.183	1.6%
CNC/PPy-2	2.0	8.017	0.186	3.2%
CNC/PPy-4	4.0	8.007	0.192	6.1%
CNC/PPy-6	6.0	8.033	0.201	10.3%
PPy-Blank	3.0	0	0.013	100.0%

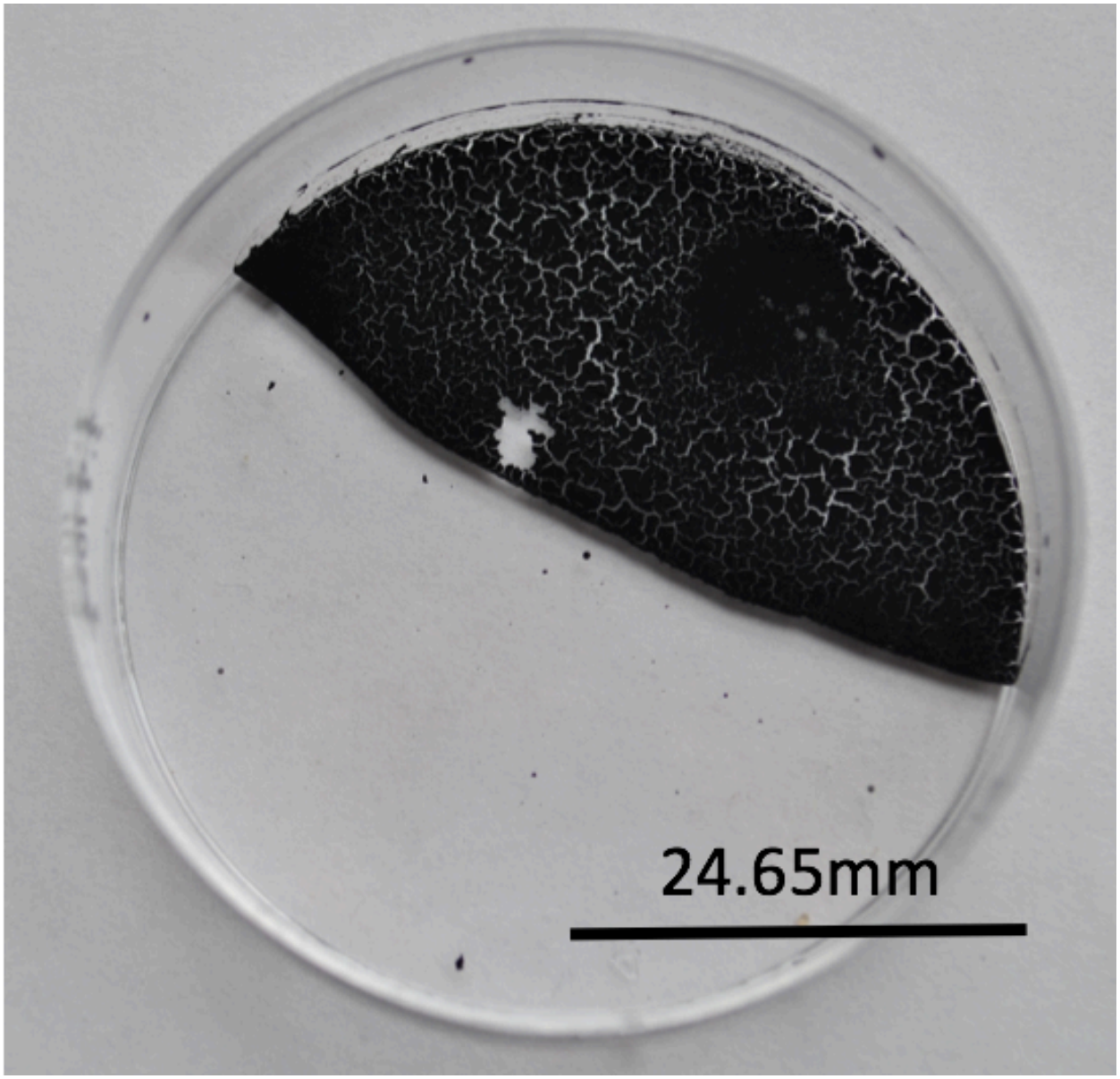

Figure 4-2 Photograph of PPy Blank

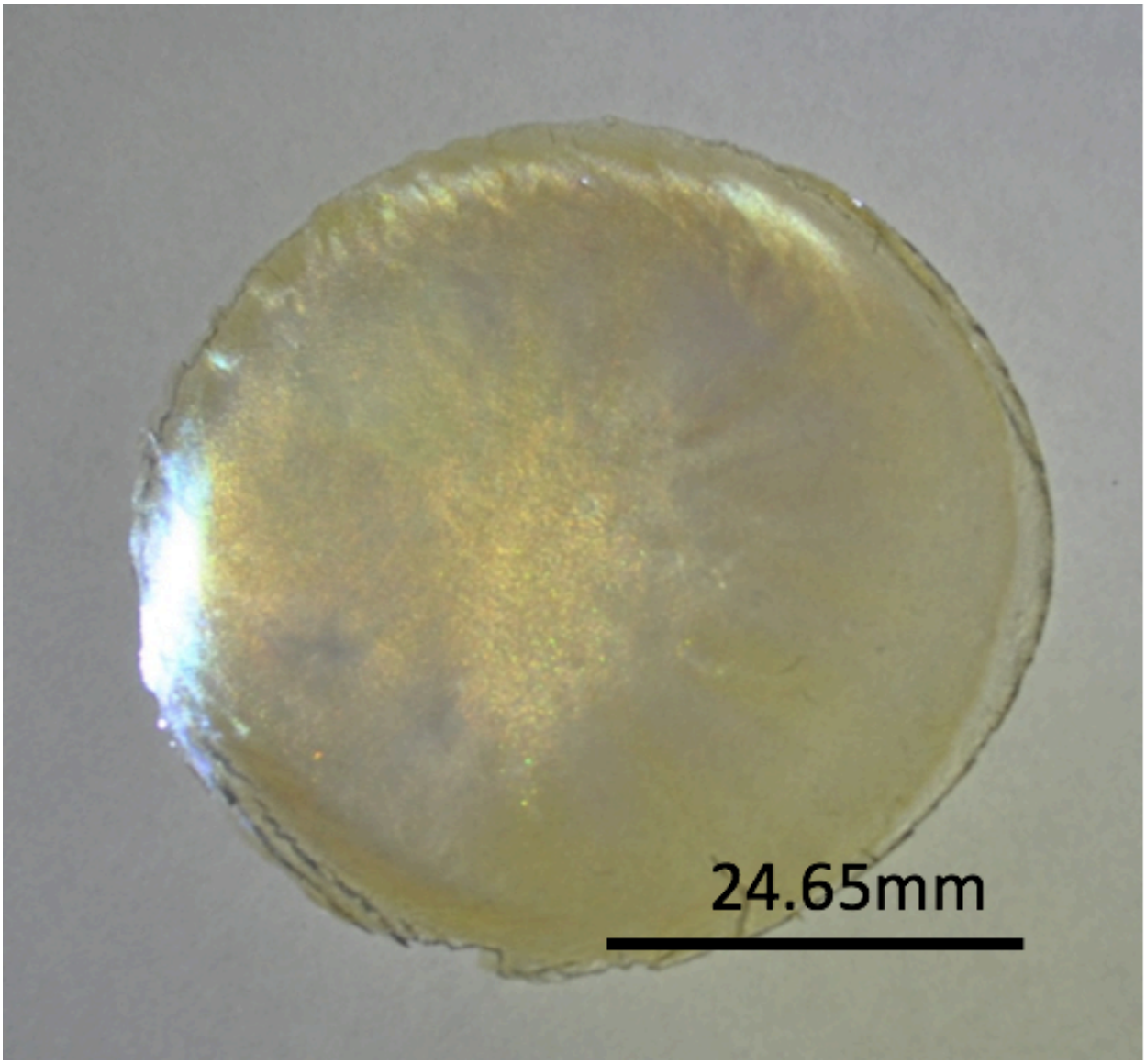

Figure 4-3 Photograph of CNC Blank removed from petri dish

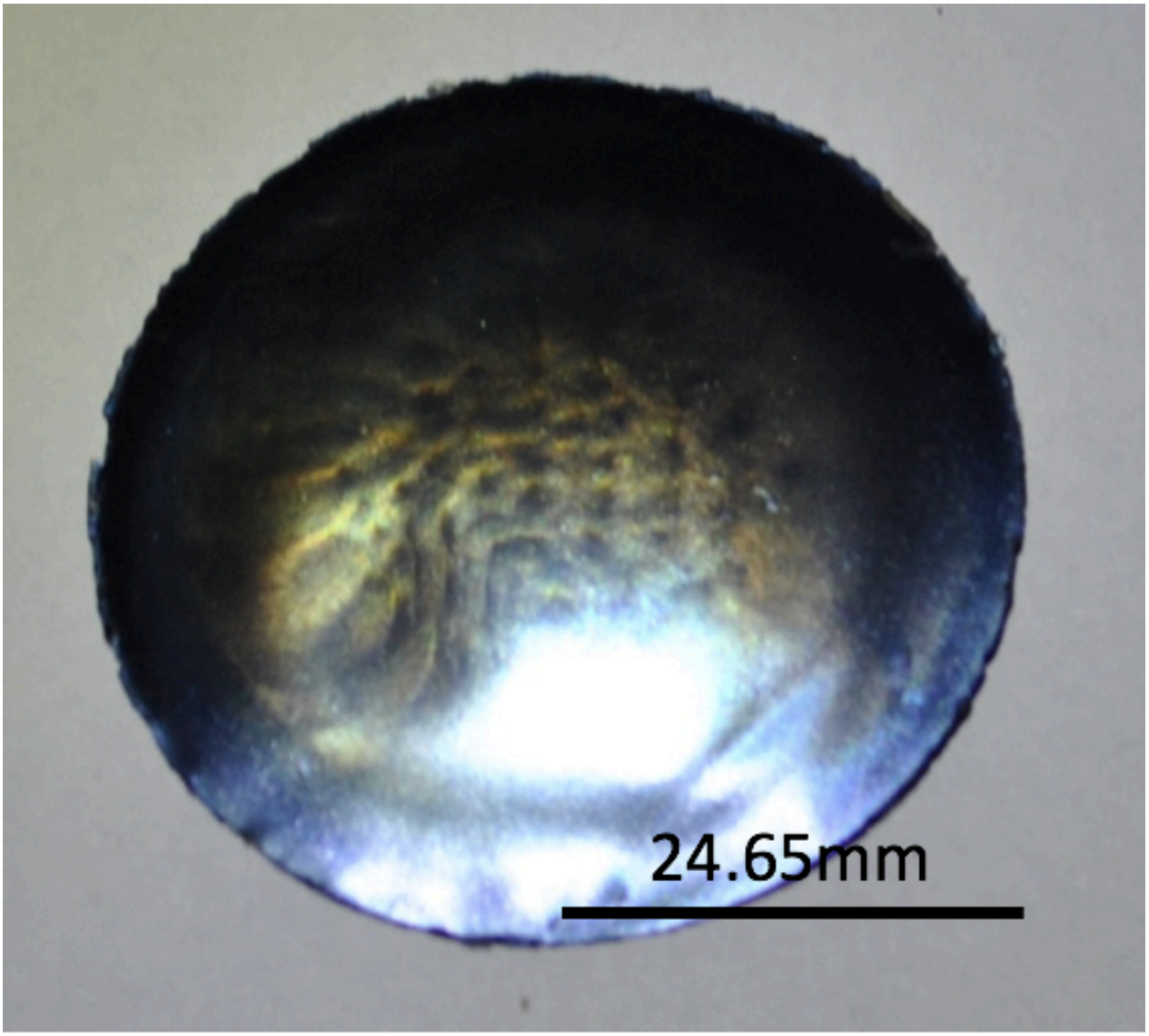

Figure 4-4 Photograph of CNC/PPy-6 removed from petri dish

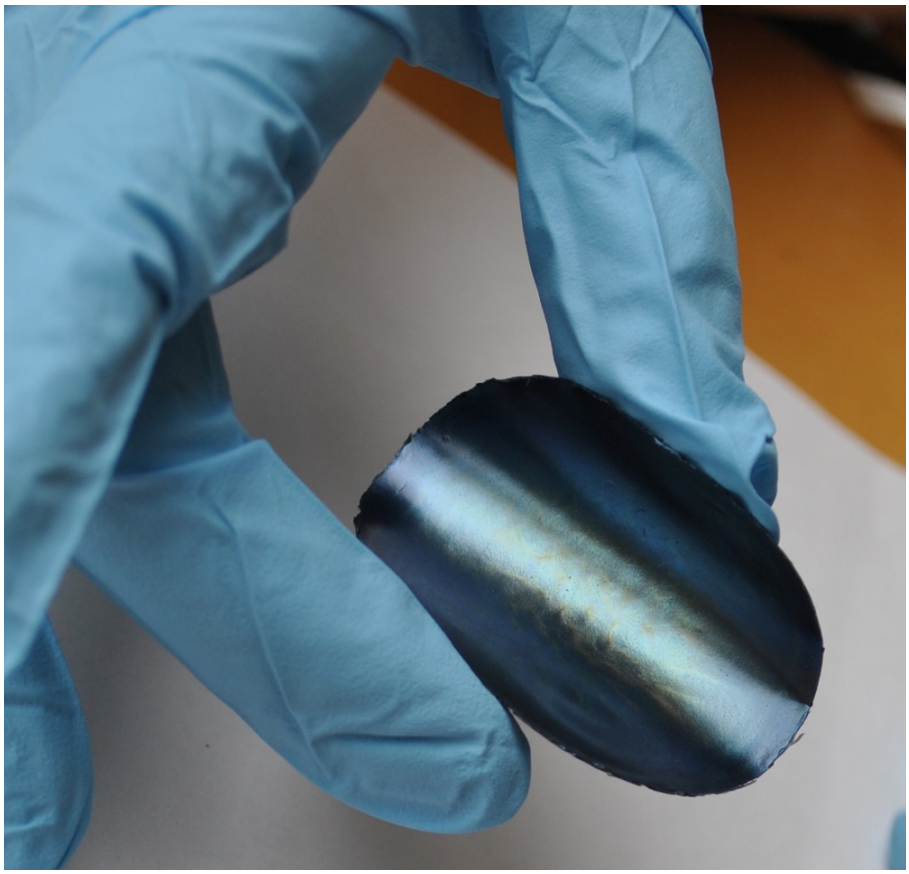

Figure 4-5 Photograph showing bending the film of CNC/PPy-6 to illustrate flexibility

4.2.2 SEM

The CNC/PPy composite films, when viewed in cross-section by SEM, did not appear visually different from the cross-section of the CNC blank film (Figure 4-9) with no PPy. The samples imaged were CNC/PPy-0.5 (Figure 4-6) and CNC/PPy-1 (Figure 4-7). Viewed at two magnifications each, the samples did not appear to be any different from each other, despite the difference in PPy loading. It is possible that imaging samples with a higher loading of Ppy would produce an image that does appear different than pure CNC films or from the low-loading films. However, the bottom of the composite films (Figure 4-8) did appear to have dried less uniformly.

On these samples, the surface looks rough, as if some layers snapped after contracting tightly when drying. Such features could not be found on the bottom of the CNC blank (Figure 4-9). When comparing CNC blank to CNC/PPy-1, the tops of the films look about the same, quite smooth. The image of the top of the CNC film highlights a single wrinkle.

The CNC blank is clearly chirally twisted, with a form that curls in one direction. Similar twisting is not observed in the CNC/PPy-1 images.

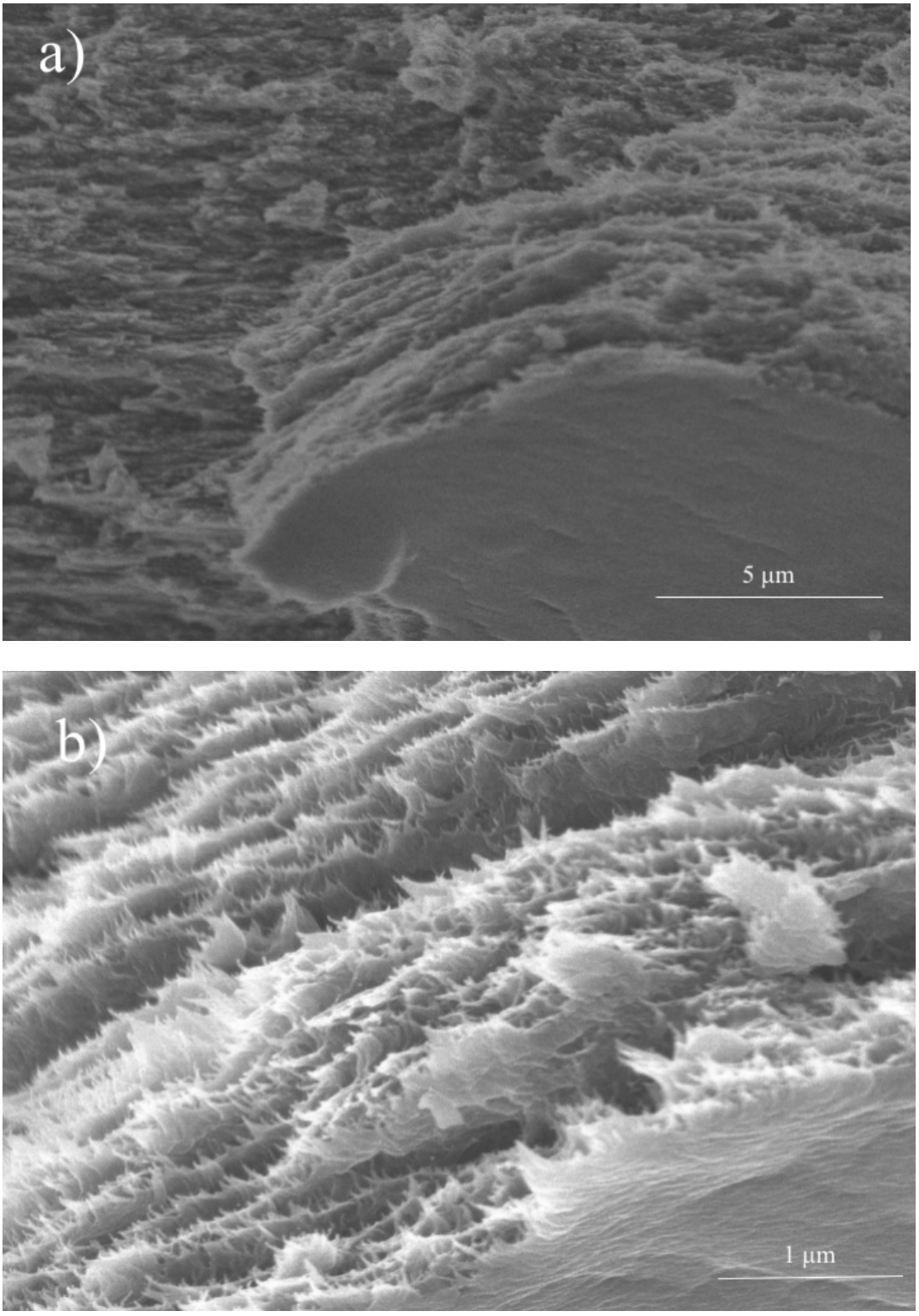

Figure 4-6 Scanning Electron Microscopy (SEM) cross-section images of CNC/PPy-0.5 at two different magnifications

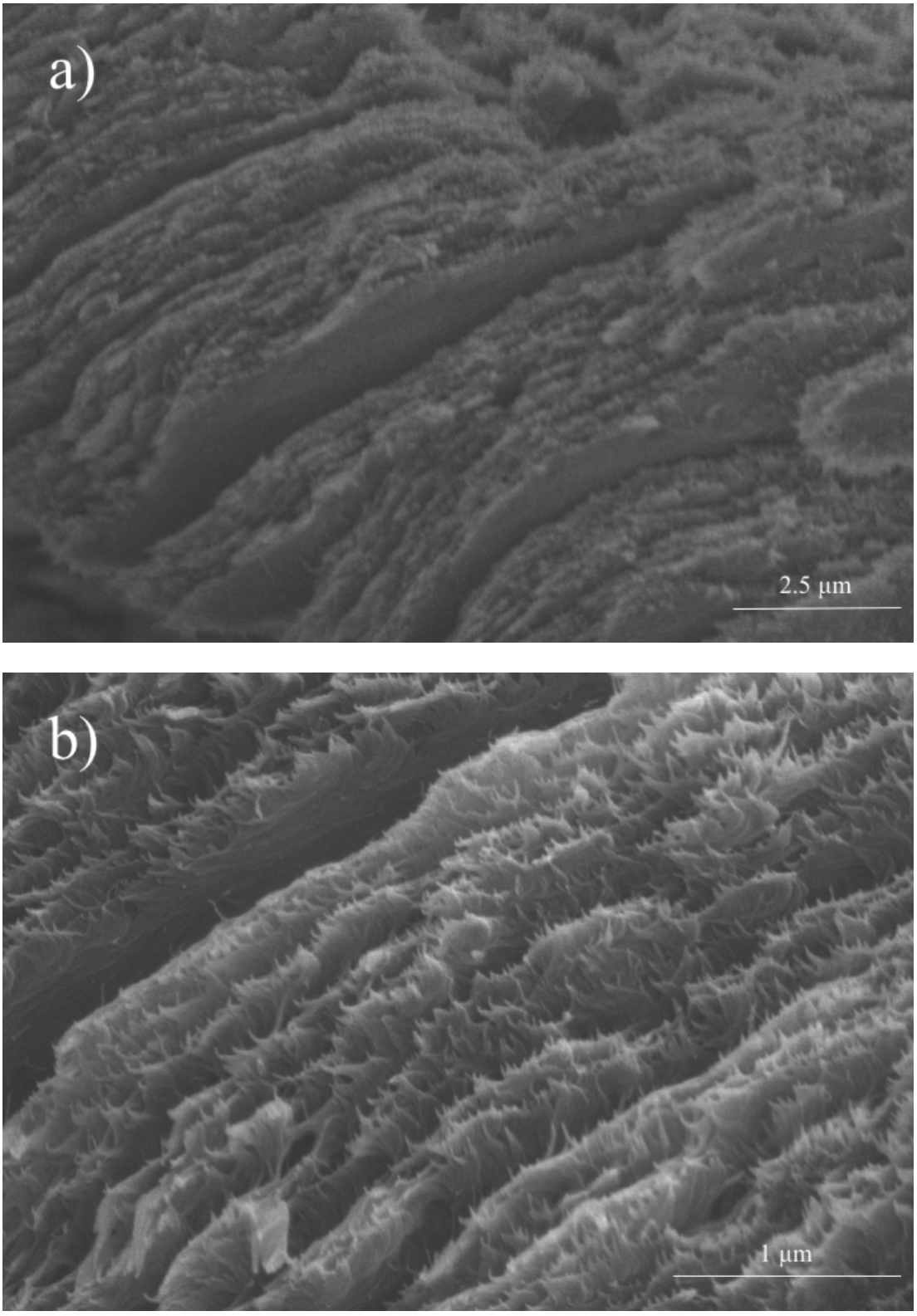

Figure 4-7 Scanning Electron Microscopy (SEM) cross-section images of CNC/PPy-1 at two different magnifications

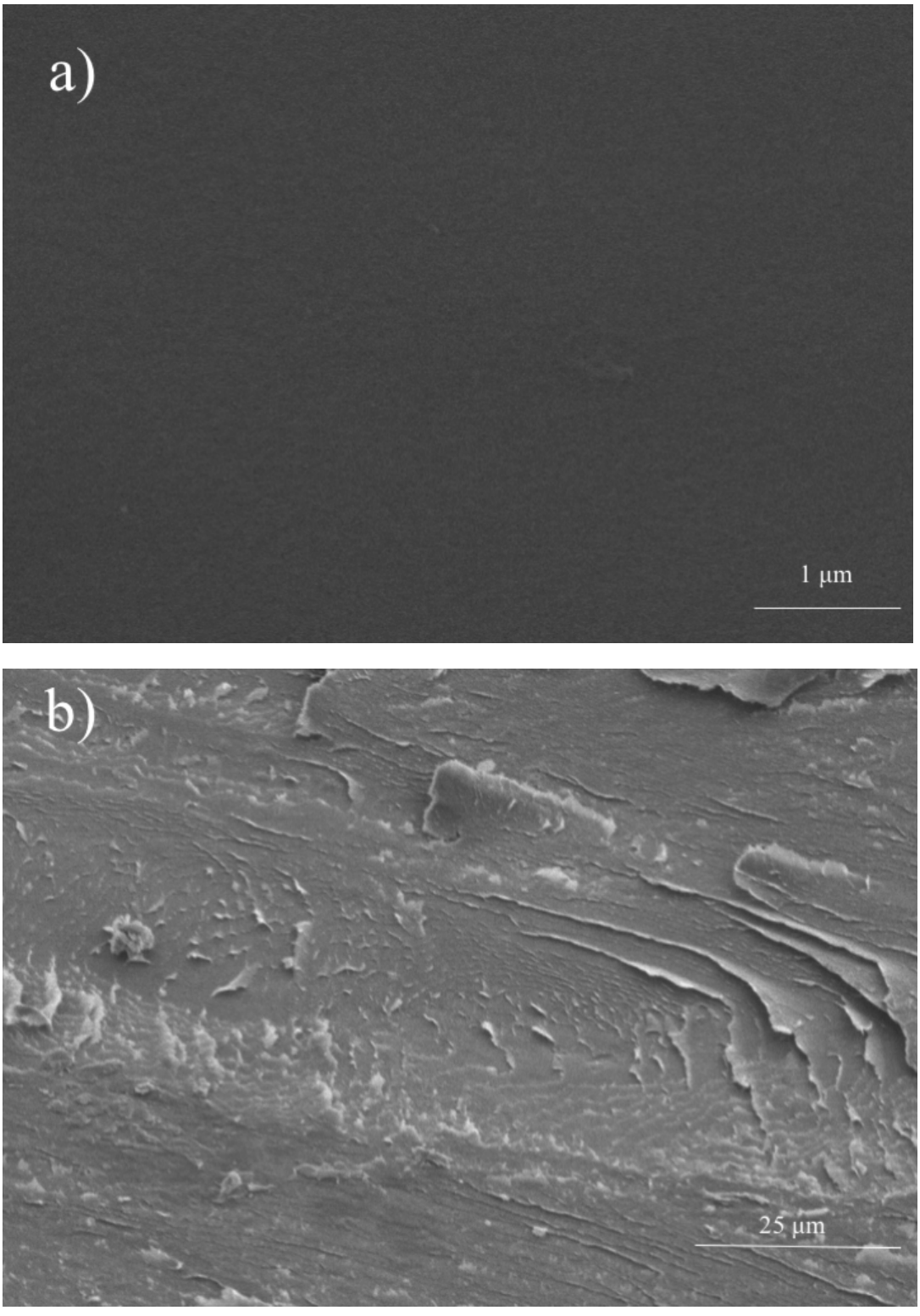

Figure 4-8 Scanning Electron Micrograph (SEM) images of CNC/PPy-1, top (a) and bottom (b) of film

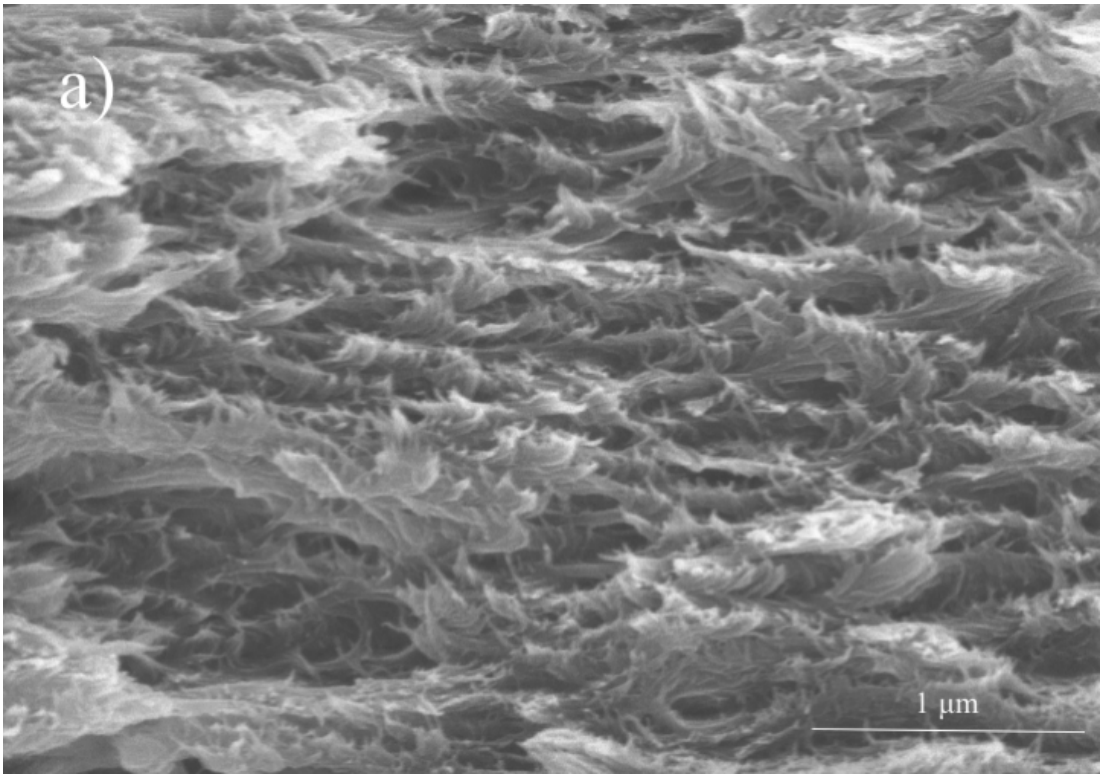

Figure 4-9 Scanning Electron Micrograph (SEM) cross-section image of CNC blank film

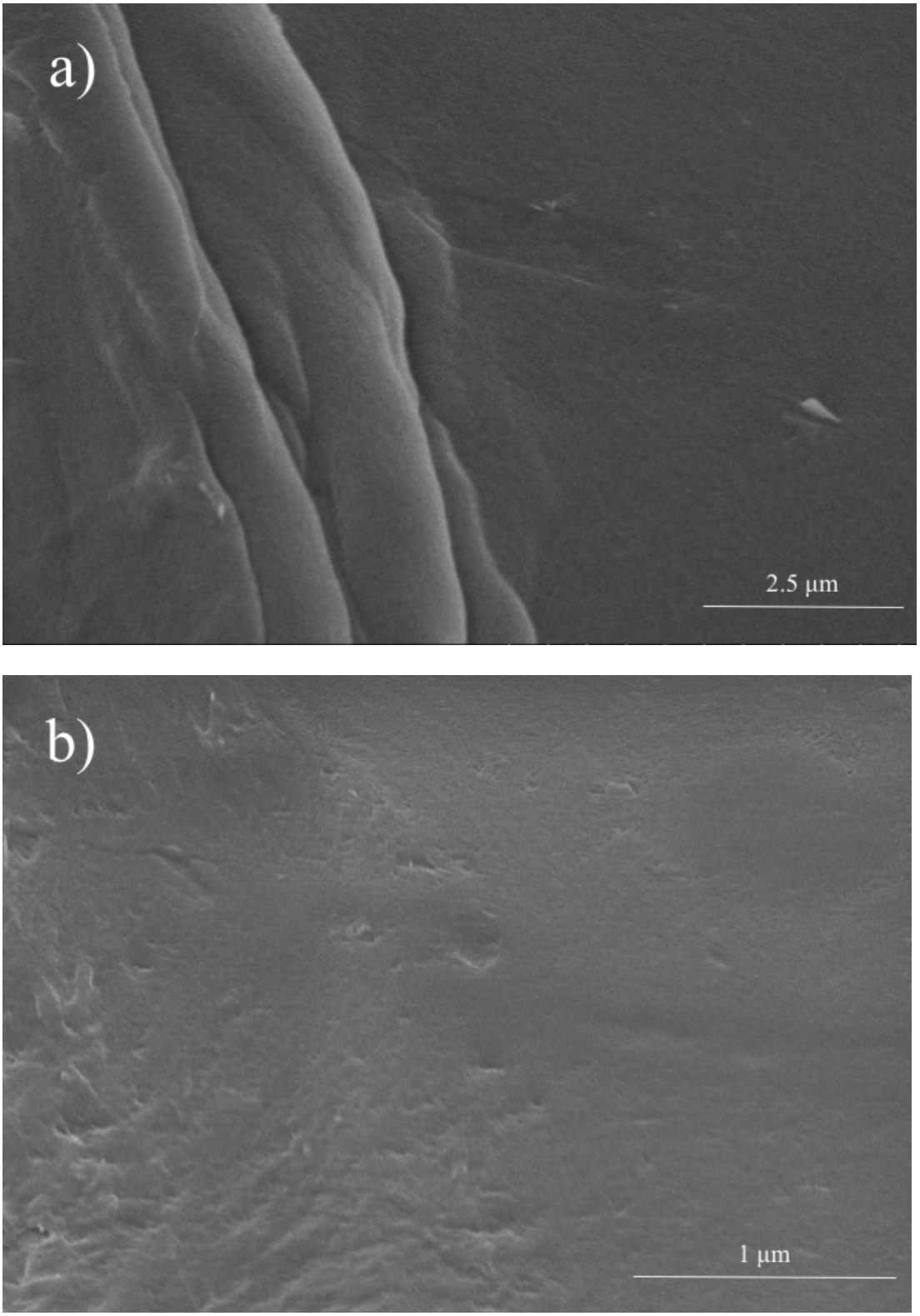

Figure 4-10 Scanning Electron Microscopy (SEM) image of CNC blank film top and bottom

4.2.3 XRD

The two blank samples and CNC/PPy-6 were characterized in film form by wide-angle X-ray diffraction. The CNC/PPy-6 film was tested, and compared to CNC-Blank and PPy-Blank (fig 4-11). The CNC-Blank turned out as expected, nearly identical to other CNC films previously tested by the MacLachlan lab at UBC. The two characteristic peaks seen for CNC result from a combination of many poorly resolved broad peaks. The CNC/PPy-6 was quite similar to the CNC blank – essentially the same peaks with higher intensity. This makes sense when taking into account results for PPy-Blank. The dried PPy appears to be amorphous, so it doesn't contribute to the crystallinity of the composite film.

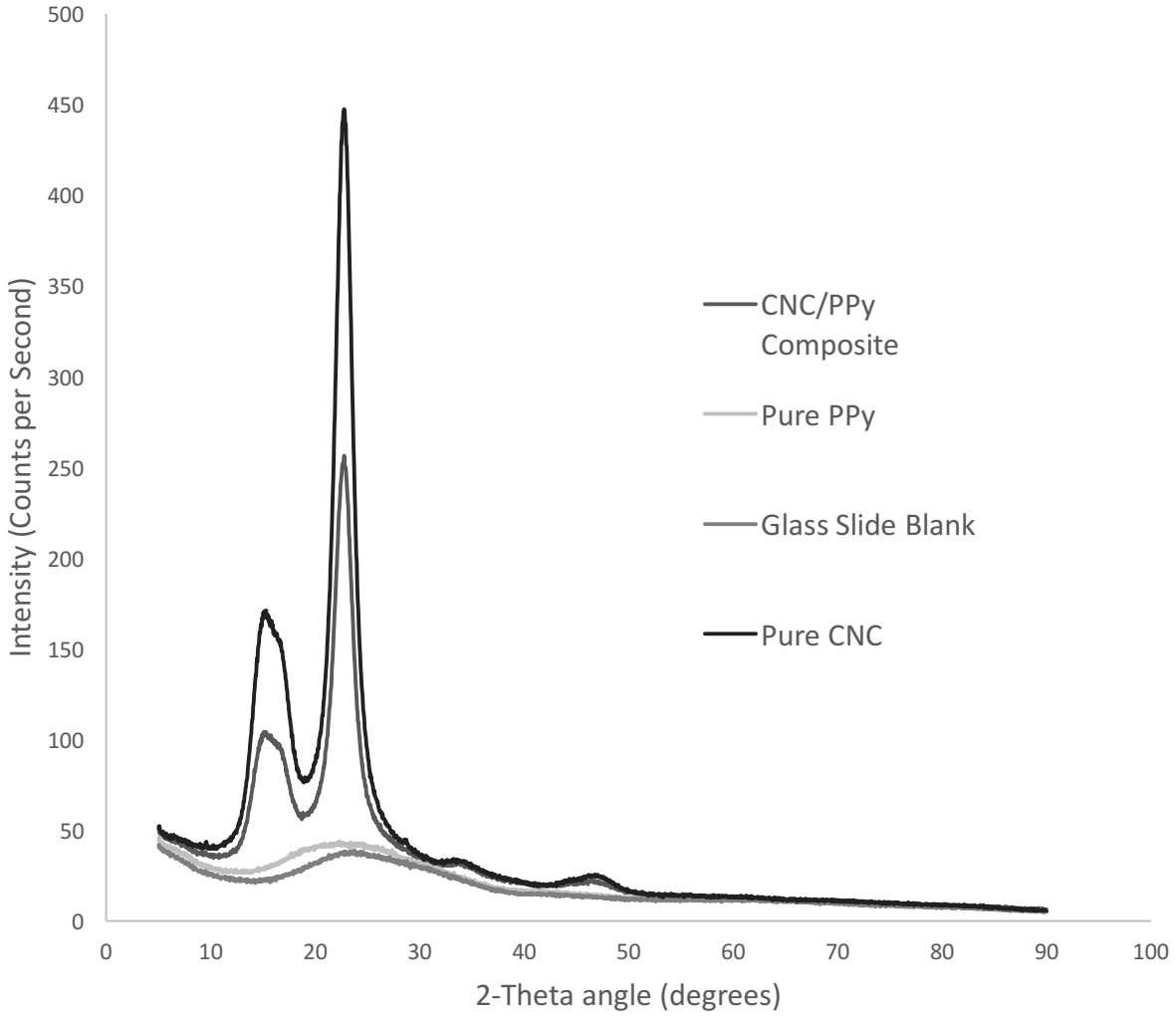

Figure 4-11 XRD data for CNC/Ppy Composite

4.2.4 CV

CNC/PPy composite was tested by cyclic voltammetry to investigate whether the films had any electrical capacitance. Small sections of film were cut with a razor, all 10 ± 1 mg. A number of different electrolytes may be used for CV. For these experiments 1 M KCl, 5 M KOH, and 1 M H_2SO_4 were chosen because they are commonly used, and have small ions that can travel through

tight pores. In order to fill the pores of samples with electrolyte, they were soaked in electrolyte at room temperature, some overnight and some for 1-2 hours. In the setup pictured, the sample is removed from electrolyte solution and placed carefully onto a stainless steel electrode (Figure 4-12). Then a circle of Whatman-1 filter paper, cut to the size of the electrode, is dipped in the same electrolyte and placed over the sample. The sample and filter paper are sandwiched between two such electrodes screwed tightly together. The filter paper prevents the two electrodes from touching. Alligator clips are used to attach the working electrode to one end of the sample holder, and the counter and reference electrodes to the opposite end (Figure 4-13).

In this case a calomel electrode was used for the reference, composed of Hg/HgCl/KCl. The counter electrode functions as a source or sink for electrons while the oxidation and reduction are performed by the working electrode. The working electrode precisely controls the current, but is not able to simultaneously measure it. The reference electrode therefore provides a constant potential against which to measure the changes throughout the test. In a potentiostat that uses stainless steel electrodes, the reference electrode is located inside the potentiostat box, and has a wire that contacts the wire used for the working electrode.

During the test, the working electrode sweeps from a specified positive potential to specified negative potential, and then back again, for as many cycles as specified. The current is measured as a function of applied potential. The sample is reduced by sweeping the current from positive to negative, then oxidized by sweeping the current back up again. During this process, ions from the electrolyte rush in and out of the pores in the sample. If the sample were a perfect conductor, the output would precisely match the input as it sweeps, resulting in a diagonal line on the output graph. But if the sample has capacitance, it will hold charge and resist the change; it will take some time for the applied potential to reduce and oxidize it on each sweep. The CV graph

of a strong capacitor will be a leaf-like shape that approaches the shape of a rectangle. The robustness of a capacitor to handle multiple charge and discharge cycles is measured by repeatedly sweeping the potential from positive to negative. If the thick leaf shape becomes flatter, the sample is losing its capacitance, and likely losing structural integrity as well. Swelling and deswelling caused by electrolyte movement contributes to breakdown of structure.

After many variations of CV tests on CNC/PPy films, it was observed that choice of sample and electrolyte, and testing conditions had some interesting effects on the shape of the output graphs. A range of 0.4 to 0.8 V tended to yield graphs that had the desired leaf-shape. Unfortunately, it was concluded that the films had no significant capacitance because the current observed with a sample was not much different from that of a "blank" test of a filter paper and electrolyte with no sandwiched sample. Although the leaf shape was present, the actual current was not significant.

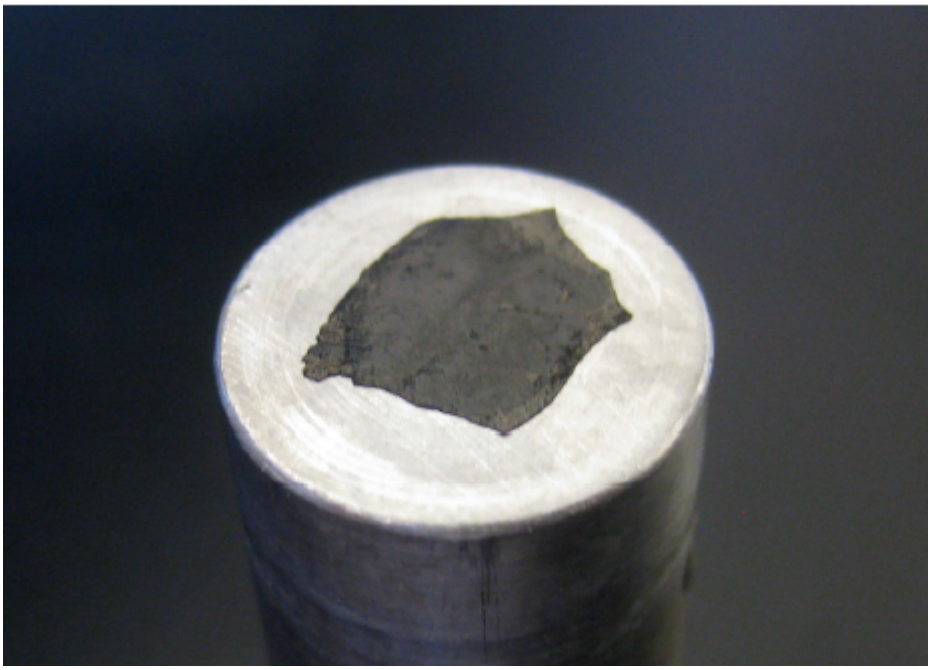

Figure 4-12 CNC/PPy composite soaked in electrolyte and placed on electrode for cyclic voltammetry

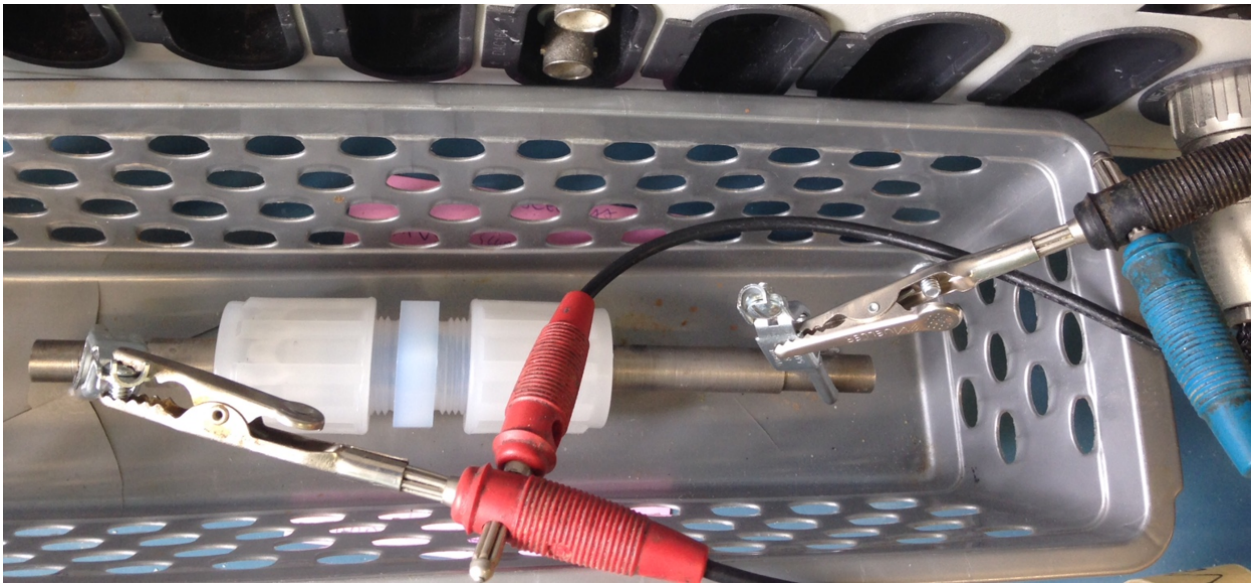

Figure 4-13 Cyclic voltammetry electrode setup

4.2.5 Conductivity

CNC/PPy samples were tested with a simple voltmeter, and found to be an insulator.

4.2.6 Hydrothermal Calcination

Because polypyrrole is rich in nitrogen, it was hypothesized that calcination of CNC/PPy films could create nitrogen-doped carbon, a useful substance in many applications, such as electrocatalysis and supercapacitors.[41,42,43] Several types of nitrogen-doped carbon materials have been reported in the literature which use polypyrrole as a nitrogen source.[44, 45, 46] The strong and flexible CNC substrate would provide the support of the structure. A hydrothermal method was attempted, heating samples under pressure in a tightly sealed bomb with exposure to water. Pieces of CNC/PPy film, around 30 mg each, were cut with a razor and placed in a small dry open vial. The vial was placed in the bomb, along with 2 mL of water outside the vial. Another similarly prepared bomb contained 2 mL of 6 M H_2SO_4 rather than water, for an acid treatment. Sealed

bombs were heated in a Thermolyne 1400 Furnace to 200 °C for four hours. Surprisingly, when weighed afterwards, the samples did not appear to have lost any mass.

Unfortunately, an EA test revealed that the calcined film had only a negligible amount of nitrogen, and was not suitable for further study.

4.3 Discussion and Future Work

The greatest success of this project is the smooth distribution of PPy through the chiral nematic CNC substrate to create an iridescent, opaque, and flexible film. It is surprising that it exhibited such poor electrochemical properties, because it does appear that the films are loaded heavily enough with PPy to guarantee lines of contact among the polymers. It is possible that the mixing with CNC solution had a detrimental effect on the conductivity of the PPy. Future investigators would be advised to look more closely into the doping of the polymer, and take care to ensure that the PPy is in a properly doped state when the films are dried. It would also be useful to establish quality-control testing of the PPy directly after synthesis.

It would also be interesting to attempt an approach inspired by the work of Nystrom et al.[36] Polymerize the polypyrrole within the CNC mixture itself, then dry a film. However, it is possible that the attachment of the polypyrrole directly to the CNCs would interfere with the chiral patterns in drying.

Chapter 5 – Conclusions

5.1 Chitosan Bioplastic

The chitosan bioplastic project successfully yielded a film that is water-resistant and reasonably strong. The films were prepared by dissolving crab-derived chitosan in acetic acid, drying to a film, then strengthening by NaOH treatment. The specific characteristics described and data tabulated in this thesis contribute to the body of literature regarding chitosan-based bioplastics.

Chitosan bioplastic made from crab chitin deacetylated for 8 h (sample CB08) was found to have a tensile strength of 93 ± 35 N/mm^2, maximum strain of 7.5 ± 2.7 %, and maximum slope of 2800 ± 1600 N/mm^2. A wide range of deacetylation times to produce the chitosan were investigated in preliminary work, guiding the decision to create large batches with 8 h and 12 h deacetylation time, for comprehensive testing. Samples in the 8 h batch were found to have superior mechanical characteristics.

Contact-angle measurements found the CB08 to be slightly hydrophilic, with a contact angle of 80 ± 4. This is in contrast to one other literature value of contact angle for chitosan films, which was found to be 98 ± 2°, slightly hydrophilic.[32] SEM images illustrated that the films dry in horizontal layers.

TGA showed that the chitosan bioplastic decomposes in two distinct phases when the temperature is ramped to 700 °C. FT-IR data indicated that the chitosan in the films had a high degree of deacetylation, with a small amount of residual proteins. A combination of information from FT-IR and XRD indicate that the films have low crystallinity.

To date, all accounts of chitosan bioplastic including this one result in simple flat films. Future work will necessarily examine techniques for fabrication of this plastic into more complex

useful shapes, such as a bag or plastic container. Other research opportunities include heat processing, molding, and adhesives.

5.2 CNC/PPy composite

A CNC/PPy blend with chiral nematic order was prepared for the first time. PPy was synthesized, mixed with CNC solution, and then dried to a film. The films are dark and opaque, yet colorfully iridescent and also flexible. Viewing through circularly polarized lenses revealed that only left-handed light was reflected by the films, indicating that the PPy does not disrupt the chiral nematic structure of the CNC template.

Though PPy itself has interesting electronic properties, the CNC/PPy blend was unfortunately found to be an insulator. No electrical conductance was observed with either CV tests or a voltmeter. The films were hydrothermally calcined in an attempt to create nitrogen-doped carbon, but the proportion of nitrogen in the product was prohibitively low. Future work should attempt to create an electronically active version of the film, particularly by taking steps to ensure that the PPy is correctly doped when the films are dried. This may be achievable by polymerizing the PPy in the presence of the CNC itself. If so, that research could lead to the first chirally-arranged conductive polymer.

References

(1) Erlich, H. *Int. Geo. Rev.* **2010**, *52*, 661-699.

(2) Campanari, S.; Augelletti, F.; Ressetti, S.; Sciubba, F.; Villano, M.; Majone, *M. Chem. Eng. J*. **2017**, *317*, 280-289.

(3) Kumar, S., Thakur, K. S. *J. Hill Agr.* **2017**, *8,* 118-129.

(4) Gurunathan, T.; Mohanty, S.; Nayak, S. K. *Composites Part A.* **2015**. *77*, 1-25

(5) Jabeen, N.; Majid, I.; Nayik, G. A. *Cogent Food & Agriculture* **2015**, *1,* Article: 1117749

(6) Saini, P.; Arora, M.; Kumar, M. N. V. R. *Adv. Drug Deliv. Rev.* **2016**, *107*, 47-59.

(7) Yarahmadi, N.; Jakubowicz, I.; Enebro, *J. Appl. Polym. Sci.* **2016**, *133*.

(8) Piemonte, V.; Gironi, F. Environ. *Prog. Sustainable Energy.* **2011**, *30,* 685–691.

(9) Aithani, D.; Mohanty, A. K. *Ind. Eng. Chem. Res.,* **2006**, *45,* 6147–6152.

(10) Luengo, J. M.; Garcia, B.; Sandoval, A.; Naharro, G.; Olivera, E. R. *Curr. Opin. Microbiol.* **2004**. *6,* 251-260.

(11) Sharma, S.; Luzinov, I. *J. Food Eng.* **2013**, *119*, 404-410.

(12) Raabe, D.; Al-Sawalmih, A.; Romano, P.; Sachs, C.; Brokmeier, H. G.; Yi, S. B.; Servos, G.; Hartwig, H. G. *Mat. Sci. Forum.* **2005**, *495*, 1665-1674.

(13) Prashanth, H.; Tharanathan, R. N. *Trends Food Sci. Tech*. **2007**, *18*, 117-131.

(14) Fernandez, J. G.; Ingber, D. E. *Macromol. Mater. Eng.* **2014**, *299*, 932–938.

(15) Benhabiles, M. S.; Salah, R.; Lounici, H.; Drouiche, *N. Food Hydrocoll.* **2012**, *29,* 48–56.

(16) Huang, Y.; Zhong, Z.; Duan, B.; Zhang, L.; Zixuan, Y.; Wang, Y.; Ye, Q. *J. Mater. Chem. B.* **2014**, *2*, 3427.

(17) Nunes, C.; Maricato, E.; Cunha, A.; Rocha, M. A. M.; Santos, S.; Ferreira, P.; Silva, M. A.; Rodrigues, A.; Amada, O.; Coimbra, J.; Silva, D.; Moreira, A.; Mendo, S.; Silva, J. A. L.; Pereira, E.; Rocha, S. M.; Coimbra, M. *Green Chem.* **2016**, *18,* 5331-5341.

(18) Gartner, C.; Lopez, B. L.; Sierra, L.; Graf, R.; Spiess, H. W.; Gaborieau, M. *Biomacromol*. **2011**, *12,* 1380-1386.

(19) Xu, J.; McCarthy, S. P., Gross, R. A. *Macromolecules* **1996**, *29,* 3436–3440.

(20) Ifuku, S.; Ikuta, A.; Egusa, M.; Kaminaka, H.; Izawa, H.' Morimoto, M.; Saimoto, H. *Carbohydr. Polym*. **2013**, *98,* 1198-1202.

(21) Jin, J.; Lee, D.; Hyeon-Gyun, I., Han, C. H.; Jeong, E. G.; Rolandi, M.; Choi, K. C.; Bae, B-S. Adv. Mater. **2016**, *28*, 5169-5175.

(22) Elsabee, M. Z.; Abdou, E. S. *Mater. Sci. Eng., C*. **2013**, *33,* 1819-1841.

(23) Tan, Y. M.; Lim, S. H.; Tay, B. Y.; Lee. M. W.; Thian, E. S. A. *J. Appl. Polym. Sci.* **2016**. doi: 10.1002/app.43796

(24) Duan, B.; Chang, C.; Ding, B.; Cai, J.; Xu, M.; Feng, S.; Ren, J.; Shi, X.; Du, Y.; *J. Mater. Chem. A,* **2013**, *1*, 1867.

(25) Quesada, J.; Sendra, E.; Navarro, C.; Sayas-Barbera, *E. Foods.* **2016**, *5,* 57.

(26) Soares, N.; Silva, P.; Barbosa, C.; Pinheiro, R.; Vincente, A. A. *J. Food Eng.* **2017**, *194,* 79-86.

(27) Lavertu, M.; Darras, V.; Buschmann, M. D. *Carbohyd. Polym.* **2012**. *87*, 1192-98.

(28) Ifuku, S.; Nogi, M.; Abe, K.; Yoshioka, M.; Morimoto, M.; Saimoto, H.; Yano, H. *Biomacromol.* **2009,** *10,* 1584-5.

(29) Nair, K. G.; Dufresne, A. *Biomacromol*. **2003**, *4,* 657-665.

(30) Wu, T. "Production and Characterization of Fungal Chitin and Chitosan. " Master's Thesis, University of Tennessee, 2004. http://trace.tennessee.edu/utk_gradthes/2254

(31) Silverstein, R.M.; Bassler, G.C.; Morrill, T.C. Spectrometric Identification of Organic Compounds. 4th ed. New York: John Wiley and Sons, **1981**.

(32) Farris, S., Introzzi, L., Biagioni, P., Holz, T., Schiraldi, A., Piergiovanni. *Langmuir* **2011**, *27*, 7563 – 74.

(33) Ateh, D. D.; Navsaria, H. A.; Vadgama, P. J.; R Soc Interface. **2006**, *3*, 741-752.

(34) Wang, G. X.; Yang, L.; Chen, Y.; Wang, J.Z.; Bewlay, S.; Lui, H. K. *Electrochim Acta.* **2005**, *50,* 4649-4654.

(35) Ilicheva, N. S.; Kitaeva, N. K.; Duflot, V. R.; Kabanova, V. I. *ISRN Polymer Science* **2012**, *2012*, Article ID 320316.

(36) Kane-Maguire, L. A. P.; Wallace, G. G. *Chem. Soc. Rev.* **2010**, *39***,** 2545–76.

(37) Shopsowitz, K. E.; Hamad, W. Y.; MacLachlan, M. J. *Angew. Chem. Int. Ed.* **2011**, *50*, 10991-95.

(38) Kelly, J. A.; Giese, M.; Shopsowitz, K. E., Hamad, W. Y., MacLachlan, M. J. *Acc. Chem. Res.,* **2014**, *47*, 1088–96

(39) Shopsowitz, K. K.; Qi, H.; Hamad, W. Y.; MacLachlan, M. J. *Nature* **2010**, *268*, 422-425.

(40) S.Mehr, S. H. M.; Giese, M.; Qi, H.; Shopsoqitz, K. E.; Hamad, W. Y., MacLachlan, M. J. Langmuir. **2013**. *29(40),* 12579-84.

(41) Nystrom, G.; Mihranyan, A.; Razaq, A.; Lindstrom, T.; Nyholm, L.; Stromme, M. *J. Phys. Chem. B*, **2010**, *114,* 4178–4182.

(42) Liew, S. L.; Thieleman, W.; Walsh, D. A.; *J. Phys. Chem. C*, **2010**, *114*,17926–33.

(43) Sasso, C.; Zeno, E.; Petit-Conil, M.; Chaussy, D.; Belgacem, M. N.; Tapin-Lingua, S.;

Beneventi, D. *Macromol. Mat. Eng*. **2010**, *295,* 934-41.

(44) Fulvio, P. F.; Jaroniec, M.; Liang, C.; Dai, S. *J. Phys. Chem. C*. **2008**, *112,* 13126–33

(45) Lin, Z.; Waller, G. H.; Lui, Y.; Lui, M.; Wong, C. *Nano Energy.* **2013**, *,* 241-248

(46) Xu, G.; Ding, B.; Nie, P.; Shen, Laifa.; Wang, J.; Zhang, X. *Chem. Eur. J.* **2013**, *19,* 12306-12.